UNIVERSITAT DE BARCELONA

ROTATING HYPERONIC NEUTRON STARS

Anna Campoy Ordaz

Master's Thesis

December call

2018/2019

Supervisors:

Àngels Ramos Gómez

Laura Tolós Rigueiro

Abstract

Neutron stars are among the most compact objects known in the Universe, with central densities several times that encountered in the center of atomic nuclei. The properties of neutron stars, such as their masses and radii, depend strongly on their internal composition, and hence the equation of state, which is still an open question. Most neutron stars are observed as pulsars, which rotate with periods as low as the millisecond. It is therefore of fundamental importance to study how rotation affects its structure and this is the main purpose of this project. To this aim, the TOV equations with the Hartle-Thorne approach for rotating neutron stars are solved for different angular velocities of rotation employing two different hadronic models: A pure nucleonic equation of state for nuclear matter, widely used in the literature, and a recently developed hyperonic equation of state, the FSU2H model, which allows two-solar-mass neutron stars with hyperons in their cores. It is found that, due to its stiffer behaviour, the FSU2H equation of state leads to smaller Keplerian frequencies than the pure nucleonic model (H&H) and, hence, the FSU2H rotating neutron stars suffer bigger deformations and reach higher moments of inertia. Particularly, the less massive neutron stars are the systems that experience the larger effects due to rotation.

Contents

Chapter 1

Introduction

A neutron stars is a type of stellar compact remnant that results from the gravitational core-collapse of an ordinary giant star with a mass in the range between 8-25$M_\odot$ during a Type-II, Ib or Ic supernova event [1].

The supernova explosion occurs when the red giant star has exhausted all its possibilities for energy production by nuclear fusion. Therefore, the pressure gradient provided by radiation is not sufficient to balance the gravitational attraction, consequently, the star becomes unstable and it eventually collapses. The inner dense regions of the star collapse first and gravitational energy is released and transferred to the outer layers, blowing them away as an expanding and fast-moving shock wave into the surrounding interstellar medium. This turns into an expanding shell of gas and dust which is observed as the supernova remnant.

Once formed, neutron stars no longer actively generate heat and cool over time. They are in hydrostatic equilibrium as the gravitational collapse is compensated by neutron degeneracy pressure and repulsive nuclear forces. Neutron degeneracy pressure is based on the Pauli exclusion principle[i]; however, this mechanism can just hold up an object until $0.7M_\odot$. For this reason, repulsive nuclear forces play a crucial role in supporting the more massive neutron stars observed.

Nevertheless, if the remnant star exceeds a maximum mass $M_{max} \sim 3M_\odot$ (Kalogera [2]), the neutron degeneracy pressure and the nuclear forces will not be enough to support the neutron star and it will collapse into a black hole.

In this context, neutron stars are the most compact objects known without an event horizon and have masses in the range between 1-2$M_\odot$. The upper limit of $2M_\odot$ has been determined in very recent measurements of neutron star binary systems (Demorest et al. [3], Antoniadis et al. [4] and Cromartie et al. [5] works). Meanwhile, their estimated range for radii goes from 10.7 km to 13.1 km (Lattimer & Prakash [6]).

[i]Quantum mechanical principle which states that two or more identical fermions cannot occupy the same quantum state simultaneously.

The properties of neutron stars, such as the mass and radius, strongly depend on their dense interior although its composition is still unknown and, hence, the equation of state (EoS) remains also undetermined. The knowledge of the EoS is a fact of great interest for many fields of Physics, ranging from nuclear physics, particle physics to astrophysics. As the true behaviour of the nuclear EoS at very high densities remains uncertain, there exist many hypothesis about the particles and phases of matter that could be possibly present in the core of neutron stars. Such models in the literature include hyperons, pion and kaon condensates, as well as deconfined quark matter.

Furthermore, the recent detection of the first direct gravitational wave event (GW170817) due to the merging of two neutron star in a binary system by LIGO and Virgo collaboration on 17 August 2017 has opened a new window of possibilities into astrophysics, dense matter, gravitation, and cosmology. This event might unlock a new path through new observables for a more detailed knowledge of the EoS at high densities for neutron stars and, as for instance their tidal deformability [7]. For example, a maximum star limit at 2.17 $M_{\odot}$ has been suggested by Margalit & Metzger [8] taking into account the measurement of the tidal deformation.

It should be emphasized that neutron stars are mostly observed as pulsars, namely neutron stars in rotation that emit periodic electromagnetic radiation. They are typically classified in terms of their period of rotation into millisecond- or second-type pulsars [9].

In consequence, the main objective of this project is to study how rotation affects neutron stars by analysing their properties after solving the hydrostatic equilibrium equations within the Hartle-Thorne approach for rotating systems. Particularly, the behaviour of the dense neutron star interior is described by an hyperonic EoS recently released by the Barcelona group [10], the so-called FSU2H model. Results are compared with those obtained with a pure nucleonic EoS widely used in the literature [11].

This purpose is achieved by first solving the non-rotating neutron stars equations and later implementing the ones for rotating neutron stars via a numerical procedure, which implies the construction and development of a FORTRAN programme, a task that has represented a personal challenge.

Nowadays, pulsars rotating with periods bigger than 700 Hz have not been observed yet, although a physics explanation preventing a more rapid rotation does not exist. For this reason, and motivated by the recently proposed sub-millisecond pulsars after the GW170817 event, we will explore different angular velocities (Ω=1000, 3000, 5000 Hz) into the neutron stars obtained by the different EoS.

Chapter 2

Theoretical framework

In this chapter, a brief summary of the historical discoveries related to neutron stars is presented. Furthermore, the structure of neutron stars is also explained in a concisely way.

2.1 Historical overview

It was not until 1932 when James Chadwick discovered the neutron. Only one year later, Walter Baade and Fritz Zwicky proposed the concept of neutron stars during their investigations of supernovae: a compact object formed by the collapse of the central core of the presupernova star [12].

This compact star made of "closely packed neutrons" would have to be degenerate and it could not generate energy after its formation; just only radiate its remaining heat through the slow process of photon diffusion.

Nevertheless, due to the small size of neutron stars in comparison with white dwarfs[i], they would be rarely observed by optical telescopes. Then, no searches for neutron stars were performed after Baade and Zick's paper.

A few years later, in 1939, Oppenheimer and Volkoff [14] and Tolman [15] derived the equations that describe the structure of a static star with spherical symmetry in General Relativity, and performed the first theoretical calculation of the equilibrium conditions of neutron stars and their properties assuming an ideal gas of neutrons at high density.

In their calculation, they found that stable static neutron stars could not have masses larger than ~ 0.75 $M_\odot$, a value much lower than the Chandrasekhar limit of white dwarfs ~ 1.44 $M_\odot$. This low value is a consequence of the simple description they made of the state of matter of the neutron star interior in terms of *non-interacting neutrons*, and it is

[i]Stellar core remnants composed mostly of electron-degenerate matter, which represent the end point of stellar evolution for main-sequence stars with masses from 0.07 to $10M_\odot$. The first white dwarf (40 Eridani B) was officially discovered in 1914 by Walter Adams [13].

an indication that the role of the nuclear forces is fundamental to determine properly the structure of these objects.

In the mid-1950s Wheeler and collaborators [16] built a more realistic neutron star matter EoS. They calculate the EoS for a non-interacting gas made of neutrons, protons and electrons under β-equilibrium conditions with respect to weak interaction processes. These authors developed a rigorous framework in which to understand compact stars, being their work of great importance even today.

In 1959 the effect of the nucleon-nucleon interaction on the EoS and structure of neutron stars was studied for the first time, finding maximum mass values of $M_{max} \sim 2M_{\odot}$ (Cameron [17]). At that time it started to be clear that, in addition to neutrons, protons and electrons, other particles such as muons, mesons or hyperons (baryons with strangeness content) could also be present in the interior of neutron stars. In spite of many efforts, the behaviour of the nuclear EoS at very high densities remained still uncertain.

Another important theoretical step was the idea that neutron superfluidity could occur in neutron star interiors, that is, a singlet-state neutron pairing which operates at subnuclear densities in the inner crust of the neutron star but disappears in the core where the neutron-neutron interaction becomes repulsive [18]. The possibility of having in the core proton pairing in a singlet-state and neutron pairing in a triplet-state was understood later. It is well known that superfluidity in nuclear matter implies important consequences for cooling and other phenomena [19].

The main processes of a strict neutron star cooling theory seems to be the emission of neutrinos and photons in a later stage. Photon cooling consists on the photon diffusion mechanism as indicated before, but the neutrino emission processes have a stronger relevance on the cooling rates of neutron stars. Neutrinos are emitted in β-decay processes Eqs. (2.1), where thermally excited neutrons or protons undergo direct or inverse beta decay and the generated neutrinos carry away energy as they escape from the star. Consequently, the star cools and the number of thermally excited nucleons drops [20].

$$\begin{aligned} \beta^{-}: &\quad n \rightarrow p + e^{-} + \bar{\nu}_e \\ \beta^{+}: &\quad p \rightarrow n + e^{+} + \nu_e \end{aligned} \tag{2.1}$$

Neutrino cooling can be used to constraint the dense matter EoS by comparing the results of theoretical cooling models with the observation of the thermal radiation from neutron stars (Bahcall and Wolf [21, 22]).

It was not until 1967 that Pacini [23] showed that rapidly rotating neutron star with a strong dipole magnetic field could transform its rotational energy into electromagnetic radiation and accelerate particles to high energies, powering in this way a surrounding nebula, like the Crab nebula (named as Crab Pulsar later on in 1968 by Pacini).

After that, on August 1967, the first radio pulsar (named PSR B1919+21) was discovered by Bell and Hewish [24]; and the name of "pulsar" was selected due to their stable signals. However, it was not until the argument of Gold [25] that pulsars were thought to be highly magnetised rotating neutron stars. Furthermore, the simultaneous discoveries of Crab and Vela pulsars in 1968 (as mentioned before), both located in supernova remnants, also confirmed the prediction of Baade and Zwicky: neutron stars are formed in supernova explosions.

Indeed, since 1968, understanding the properties of neutron stars was a matter of primordial importance and a lot of theoretical work was developed. In 1971, the discovery of pulsating compact X-ray sources (X-ray pulsars) stimulated this scenario even further. Those sources were believed to come from a neutron star in a close binary system which is accreting matter from its ordinary companion star [26].

Another important step in the history of neutron stars was the observation of the first binary pulsar (PSR J1913+16) by Hulse and Taylor in 1974 [27]. During the next years, several satellites were launched in order to observe neutron stars down to the last detail.

A last historical surprise about neutron stars has been the very recent first direct detection of gravitational waves from the merger of two neutron stars in 2017 [7], which has shaken up the entire physics' world anew.

2.2 Structure of neutron stars

Neutron stars are supported against gravitational collapse mainly by the neutron degeneracy pressure, as mention in the previous section. Having masses of the order of 1-2$M_\odot$ and radii within the range 10-13 km, an average density of the order of $\sim 10^{14}$ g/cm^3 is required. However, the internal structure of these objects can be described as an "onion" with a wide range of densities into their different shells (Figure 2.1).

The *atmosphere* is the most external region and constitutes the thin layer, having a variation of its thickness from $\sim$ 10 cm in hot neutron stars to $\sim$ mm in cold ones. The densities in the atmosphere are in the range $n \leq 10^6$ g/cm^3. It is a plasma layer where matter is formed by atoms of heavy nuclei, mainly nuclei around the iron mass number, distributed in a lattice in order to minimise the Coulomb energy.

The observed thermal spectrum of the neutron stars comes from this region and, although the theoretical study of neutron stars atmospheres has been carried out by many authors, the current models are still incomplete due to some uncertainties. The main problems that need to be solved are the difficulty of the calculation of the EoS, the ionisation equilibrium and the spectral opacity of the atmospheric plasma (see ref. [28] for a detailed review).

Then, we find the *crust* which is formed by the *outer* and *inner crust*, having a total thickness of $\sim$ 1 km and contributing only to a few percent of the total mass of the neutron star.

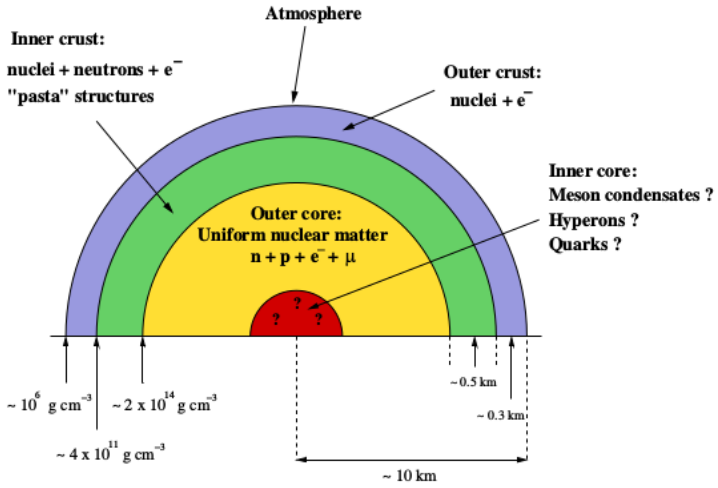

Figure 2.1: A schematic figure showing the layered structure of a neutron star. The different regions are not drawn in scale. Image from [1].

The *outer crust* is a solid region where atoms are ionised and the matter consists of a Coulomb lattice of nuclei embedded in a gas of free ultrarelativistic electrons at densities $n > 10^6$ g/cm^3. This lattice is in β-equilibrium with the strongly degenerate electron gas.

Once we start moving towards the interior of the star, still at the *outer crust*, the increase of the average density induces electron capture processes [Eq. (2.2)] and inverse β-decay processes [Eq. (2.3)] on the lattice's nuclei thus becoming the *outer crust* more and more neutron-rich (direct β-decays are inhibited).

$$\begin{aligned} e^- \ + \ {}^A Z \ &\rightarrow \ {}^A(Z-1) \ + \ \nu_e \\ e^- \ + \ p \ &\rightarrow \ n \ + \ \nu_e \end{aligned} \tag{2.2}$$

$$\begin{aligned} \bar{\nu_e} \ + \ {}^A Z \ &\rightarrow \ {}^A(Z-1) \ + \ e^- \\ \bar{\nu_e} \ + \ p \ &\rightarrow \ n \ + \ e^- \end{aligned} \tag{2.3}$$

When the density reaches a value $n = n_{drip} \sim 4{\times}10^{11}$ g/cm^3, nuclei cannot support the neutron excess and start to emit neutrons that can only occupy the levels in the continuum which are the ones available. Consequently, the nuclear "drip out" starts and this neutron drip limit defines the border between the *outer* and the next layer: the *inner crust*.

The *inner crust* can be about one kilometre thick and the density in this region ranges from n_{drip} up to $\sim 0.5 n_0$[ii]. As we have passed the drip density limit, neutrons have dripped out and formed a neutron gas coexisting with the nuclei. Hence, the *inner crust*'s matter

[ii] n_0 is the nuclear saturation density and has a value of $2.7{\times}10^{14}$g/cm^3 $\simeq 0.16$ fm^{-3}.

consists on a mixture of very neutron-rich nuclei arranged in a Coulomb lattice, electron and free neutrons which are expected to be paired in the s-wave by the nuclear residual interaction and, therefore, to form a superfluid [1].

In addition, due to the competition between the nuclear and Coulomb forces, nuclei would lose their spherical shapes and would adopt more exotic topologies; giving, as a result, the so-called "nuclear pasta" phase whose existence and relevance are not clear yet. Even though, recent works have provided some hints. Pons et al. [29] may have given the first observational evidence for an amorphous *inner crust* by showing that a highly resistive innermost layer limits the spin period of isolated X-ray pulsars. Meanwhile, Newton et al. [30] suggested that a high degree of disorder is needed in the *inner crust* by comparing the calculations of the magnetic field decay of neutron stars and their corresponding observational spin evolution, which may also provide the evidence of "nuclear pasta".

The *outer core* starts at densities of about $\sim 10^{14}$ g/cm^3, when the nuclear clusters dissolve into their constituents, neutrons and protons. Then matter roughly consists of an homogeneous quantum fluid of nucleons and electrons in beta equilibrium. Specifically, matter is mainly composed of p-wave superfluid neutrons with a smaller concentration of s-wave superconducting protons and normal electrons (in the same amount of protons in order to achieve charge neutrality), and muons which appear as soon as their chemical potential equals that of the electron ($\mu_\mu = \mu_e$).

Lastly, the densities of this region go in the range $0.5n_0 \leq n \leq 2n_0$ and it has a thickness of several kilometres. For low-mass neutron stars, whose central densities are found to be less than 2-3n$_0$, the *outer core* actually constitutes the entire core of the object. But for high-mass neutron stars, the central densities could easily be in the range $n \geq 2n_0$ forming the innermost layer.

So, finally, the *inner core* is several kilometres of thickness and its composition is still unknown. However, there are some speculative ideas. The hypotheses go from hyperonic matter, pion or kaon condensates to deconfined quark matter.

In any case, this project would focus on purely baryonic matter phase at the centre of the star. Therefore, nucleonic and hyperonic models used in this work are briefly explained in the next chapter.

Chapter 3

Equations of state of β-stable neutron star matter

The EoS is a relation in which thermodynamic variables describes the state of matter; even though, its determination is still one of the main problems that need to be solved. For that reason, one can find in the literature many EoSs obtained from different approaches (Mean-Field or Microscopic model) using diverse types of interactions (non-relativistic, relativistic, effective theories or/and meson-exchange based) with or without many-body forces.

Consequently, in this chapter, we are going to explain the purely baryonic EoSs used in this project and their respective formalisms and parameterizations. The H&H model is based on nucleonic matter meanwhile FSU2H EoS incorporates hyperonic matter.

However, one should understand first how matter remains in equilibrium in neutron stars.

3.1 Beta-stability conditions

First of all, as previously mentioned in Section 2.2, neutron stars are not only made of neutrons. In order to determine its chemical composition, one should impose some conditions: charge neutrality

$$\sum_{i=1}^{L} q_{l_i} n_{l_i} + \sum_{i=1}^{B} q_{b_i} n_{b_i} = 0 \ , \tag{3.1}$$

and conservation of the baryonic density

$$n_B = \sum_{i=1}^{B} B_{b_i} n_{b_i} \ , \tag{3.2}$$

being b_i and l_i the baryon and lepton indexes respectively, that run over all types of baryons (B) and leptons (L). Meanwhile B_{b_i} refers to the corresponding baryonic number and the products $q_{b_i} n_{b_i}$ and $q_{l_i} n_{l_i}$ describe the charge density of baryons and leptons, being q_{b_i} and q_{l_i} the proper charge number.

Also, neutron stars are in equilibrium against weak interaction processes (β decay and lepton capture) described by:

$$b_1 \to b_2 + l + \bar{\nu}_l \qquad\qquad b_2 + l \to b_1 + \nu_l \tag{3.3}$$

where b_1 and b_2 represent two different types of baryons, l refers to a lepton, and ν_l and $\bar{\nu}_l$ are the respective leptonic neutrino and anti-neutrino.

If only the β-decay process was taking place, the decay of a free baryon would be halted by the presence of the second baryon and lepton; as baryons have already occupied their lowest levels of their corresponding Fermi seas. Therefore, the Pauli exclusion principle would prevent the decay reaction. The equilibrium is obtained by the lepton capture reaction, imposing charge and baryon number conservation [see Eqs. (3.1) and (3.2)]. Notice that lepton number conservation is not applied since the free path of a neutrino in a neutron star is bigger than its typical radius (~ 10 km), assuming throughout that neutrinos escape freely out of the star.

Once we have explained the two conserved charges of cold neutron stars, as a way of finding its equilibrium state, we proceed minimising the total energy density of the system constrained by the equilibrium conditions previously mentioned employing the method of Lagrange multipliers:

$$\begin{aligned} F(n_{b_1}, n_{b_2}, ..., n_{b_B}, n_{l_1}, n_{l_2}, ..., n_{l_L}) = \varepsilon(n_{b_1}, n_{b_2}, ..., n_{b_B}, n_{l_1}, n_{l_2}, ..., n_{l_L}) \\ + \alpha \left(n_B - \sum_{b_i} B_{b_i} n_{b_i} \right) + \beta \left(\sum_{b_i} q_{b_i} n_{b_i} + \sum_{l_i} q_{l_i} n_{l_i} \right) \end{aligned} \tag{3.4}$$

The quantities α and β are the corresponding Lagrange multipliers. In coherence, the subscripts b_i and l_i run over B and L respectively.

Now, the minimisation of the energy of the system is given by:

$$\begin{aligned} &\frac{\partial F}{\partial n_{b_1}} = 0, \ ..., \ \frac{\partial F}{\partial n_{b_B}} = 0, && \frac{\partial F}{\partial n_{l_1}} = 0, \ ..., \ \frac{\partial F}{\partial n_{l_L}} = 0, \\ &\frac{\partial F}{\partial \alpha} = 0, && \frac{\partial F}{\partial \beta} = 0. \end{aligned} \tag{3.5}$$

Then, keeping in mind that the chemical potential of a species "i" is just $\mu_i = \partial\varepsilon/\partial n_i$, we obtain a set of general equations for all type of baryons and leptons respectively:

$$\mu_{b_i} - B_{b_i}\alpha + q_{b_i}\beta = 0, \qquad i = 1, ..., B; \tag{3.6}$$
$$\mu_{l_j} + q_{l_j}\beta = 0, \qquad j = 1, ..., L. \tag{3.7}$$

In general, N species and 2 Lagrange multipliers give N+2 equations, what means B+L equations from Eq. (3.5) and the 2 equations from the conserved charges [Eqs. (3.1) & (3.2)]. Consequently, the first B+L equations allow to write the unknown chemical potentials in terms of the two chosen ones (there are as many independent chemical potentials as conserved charges), thus helping us to eliminate the Lagrange multipliers α and β and determine the composition of beta-stable neutron star matter.

For convenience, we develop the baryonic equation for the neutron and the leptonic equation for the electron:

$$\frac{\partial F}{\partial n_n} = \mu_n - \alpha = 0 \qquad \longrightarrow \qquad \mu_n = \alpha \tag{3.8}$$
$$\frac{\partial F}{\partial n_e} = \mu_e - \beta = 0 \qquad \longrightarrow \qquad \mu_e = \beta. \tag{3.9}$$

Therefore, the chemical potential of any particle can be obtained in terms of μ_e (associated with charge neutrality) and μ_n (associated with conservation of the total baryonic density) as a linear combination weighted by the baryon number and the electric charge of the particle as

$$\mu_{b_i} = B_{b_i}\mu_n - q_{b_i}\mu_e, \qquad i = 1, ..., B; \tag{3.10}$$
$$\mu_{l_j} = -q_{l_j}\mu_e, \qquad j = 1, ..., L. \tag{3.11}$$

Finally, from these equations, it is clear that not only the weak interaction rules the composition of neutron star matter, being the responsible for the conversion processes of one species into another, but also the strong interaction plays a role as it determines the explicit value of the chemical potentials of the baryons.

In brief, the solution of these last equations determines the composition of beta-stable matter at its ground state for a given density and type of particle.

3.2 General Equations-of-State considerations

Before starting with the explanation for the purely baryonic models used in this project, one needs to introduce some basic concepts.

The pressure P is defined as

$$P = \rho^2 \frac{\partial \mathscr{E}}{\partial \rho} = \rho \frac{\partial \varepsilon}{\partial \rho}, \tag{3.12}$$

where $\mathscr{E}$ refers to the energy per baryon which has units of MeV, while the number density ρ is in units of fm^{-3}. The energy density correspond to ε and has dimensions of $\mathrm{MeV/fm}^3$ as the pressure P.

In the calculations of properties of neutron star matter in β-equilibrium, one needs the calculation of the energy per baryon $\mathscr{E}$ for several proton fractions x_p, which correspond to the ratio of protons as compared to the total nucleon number (Z/A). It is defined as

$$x_p = \frac{\rho_p}{\rho} = \frac{\rho_p}{\rho_p + \rho_n}, \tag{3.13}$$

where $\rho = \rho_p + \rho_n$ is the total baryonic density if neutrons and protons are the only baryons present, which is one of the charges that must be conserved as already mentioned. Note that $\rho_p = x_p \rho$ and $\rho_n = (1 - x_p)\rho$.

Then, the total Fermi momentum k_F and the Fermi momenta k_{F_p}, k_{F_n} for protons and neutrons are related to the total baryon density (or nucleon density) by:

$$\rho = \frac{2}{3\pi^2} k_F^3 = x_p \rho + (1 - x_p)\rho = \frac{1}{3\pi^2} k_{F_p}^3 + \frac{1}{3\pi^2} k_{F_n}^3. \tag{3.14}$$

The energy per baryon is thus labelled as $\mathscr{E}(\rho, x_p)$, referring $\mathscr{E}(\rho, 0)$ to the energy per baryon for pure neutron matter (PNM) while $\mathscr{E}(\rho, 1/2)$ is the corresponding value for symmetric nuclear matter (SNM). An important ingredient in the discussion of any EoS is the so-called symmetry energy, defined as the difference in energy for symmetric nuclear matter and pure neutron matter:

$$\mathscr{S}(\rho) = \mathscr{E}(\rho, 0) - \mathscr{E}(\rho, 1/2). \tag{3.15}$$

Expanding the energy per baryon only in the proton concentration x_p about the value of the energy for SNM ($x_p = 1/2$), we obtain:

$$\mathscr{E}(\rho, x_p) = \mathscr{E}(\rho, 1/2) + \frac{1}{2} \frac{d^2 \mathscr{E}}{dx_p^2}(\rho)(x_p - 1/2)^2 + ... \simeq \mathscr{E}(\rho, 1/2) + 4\mathscr{S}(\rho)(x_p - 1/2)^2, \tag{3.16}$$

where the term $\frac{d^2\mathscr{E}}{dx_p^2}$ is associated with the symmetry energy $\mathscr{S}(\rho)$ by the empirical mass formula and the higher-order derivatives are assumed to be small.

From the definition of the chemical potential and imposing the known beta-equilibrium conditions, we are able to express proton and neutron chemical potentials in terms of the symmetry energy and proton fraction:

$$\begin{aligned}
\mu_p &= \frac{\partial\varepsilon}{\partial\rho_p} = \frac{\partial(\mathscr{E}\rho)}{\partial\rho_p} = \frac{\partial(\mathscr{E}\rho)}{\partial\rho}\frac{\partial\rho}{\partial\rho_p} + \frac{\partial(\mathscr{E}\rho)}{\partial x_p}\frac{\partial x_p}{\partial\rho_p} = \left[\frac{\partial\mathscr{E}}{\partial\rho}\rho + \mathscr{E}\right] + (1-x_p)\frac{\partial\mathscr{E}}{\partial x_p} \\
\mu_n &= \frac{\partial\varepsilon}{\partial\rho_n} = \frac{\partial(\mathscr{E}\rho)}{\partial\rho_n} = \frac{\partial(\mathscr{E}\rho)}{\partial\rho}\frac{\partial\rho}{\partial\rho_n} + \frac{\partial(\mathscr{E}\rho)}{\partial x_p}\frac{\partial x_p}{\partial\rho_n} = \left[\frac{\partial\mathscr{E}}{\partial\rho}\rho + \mathscr{E}\right] - x_p\frac{\partial\mathscr{E}}{\partial x_p} \\
\Rightarrow \mu_n - \mu_p &= -\frac{\partial\mathscr{E}}{\partial x_p} = 4\mathscr{S}(\rho)(1-2x_p).
\end{aligned} \tag{3.17}$$

Finally, other properties of interest in the characterisation of EoSs are the incompressibility modulus K at non-zero pressure:

$$K = 9\frac{\partial P}{\partial\rho}, \tag{3.18}$$

and the sound speed v_s, which depends also on the density of the nuclear medium thorugh the relation:

$$\left(\frac{v_s}{c}\right)^2 = \frac{dP}{d\varepsilon} = \frac{dP}{d\rho}\frac{d\rho}{d\varepsilon} = \left(\frac{K}{9(m_nc^2 + \mathscr{E} + P/\rho)}\right). \tag{3.19}$$

The tracking of the dependence on density of v_s is important, since a superluminal behaviour can occur at higher densities for some EoSs.

3.3 Nucleonic matter: H&H model

Heiselberg and Hjorth-Jensen [11] detailed a simple parameterization of a non-relativistic nuclear matter model including three-body forces at temperatures much lower than the typical Fermi energies (T=0).

The binding energy per nucleon in nuclear matter used by Heiselberg and Hjorth-Jensen (H&H) is adopted to be the sum of a compressional and a symmetry term:

$$\mathscr{E} = E_{comp}(n) + \mathscr{S}(n)(1-2x_p)^2 = \mathscr{E}_0 u \frac{u-2-\delta}{1+\delta u} + \mathscr{S}_0 u^\gamma (1-2x_p)^2 \ , \tag{3.20}$$

being $\mathscr{S}(n)$ the symmetry energy and x_p is the proton fraction, defined as $x_p = n_p/n$. The ratio of the baryon density to nuclear saturation density corresponds to $u = n/n_0$.

The first term is parametrized in order to reproduce the saturation density, binding energy and compressibility of symmetric nuclear matter. The binding energy per nucleon at saturation density is taken to be $\mathscr{E}_0$=-15.8 MeV (without Coulomb energies). The introduction of δ parameter is justified by applying the condition that the sound speed $v_s^2 = \partial P/\partial\varepsilon$ does not exceed the speed of light. A value of δ=0.2 is chosen in order to avoid having a EoS that becomes superluminical at high densities. In agreement with the experimental value, the compressibility related to the first term is found to be $K_0 = 18\mathscr{E}_0/(1+\delta) \simeq 200$ MeV. For the second term (the symmetry energy term), the best fit gives $\mathscr{S}_0$=32 MeV and γ=0.6.

In neutron star matter, one needs to impose beta-stable conditions. In the H&H model, charge neutral uniform matter is made mainly of neutrons, protons, electrons and muons, and their composition is determined by the requirements of chemical and electrical equilibrium as exposed in Section 3.1. From Eqs. (3.3) and (3.11), the following conditions for matter in β-equilibrium with only nucleonic degrees of freedom are obtained:

$$\mu_n = \mu_p + \mu_e \qquad\qquad n_p = n_e. \tag{3.21}$$

Notice that neutrinos are not included in the conditions for β-stable matter as already mentioned before.

Moreover, assuming ultra-relativistic electrons ($p_e \sim 100$ MeV), their chemical potential is found to be:

$$\mu_e = \frac{1}{n}\frac{\partial\varepsilon}{\partial x_p} = k_{F_e} = (3\pi^2 n_e)^{1/3} = (3\pi^2 n_p)^{1/3} = 4\mathscr{S}(n)(1-2x_p). \tag{3.22}$$

The dependence of the electron chemical potential on the symmetry energy and proton fraction (last term of Eq. (3.22)) is found by using the expressions for the proton and neutron chemical potentials [Eq. (3.17)] from the previous section, keeping in mind the β-equilibrium conditions [Eq. (3.22)]. Therefore, from these results, one can conclude that the symmetry energy $\mathscr{S}(\rho)$ has a important role in studies of neutron star matter in beta-equilibrium.

Therefore one is able to express the proton fraction in terms of the symmetry energy:

$$nx_p = \frac{(4\mathscr{S}(n)(1-2x_p))^3}{3\pi^2}. \tag{3.23}$$

In the case of the H&H parametrization, the energy per particle for β-stable matter turns out to be given analitically by:

$$\mathscr{E} = \mathscr{E}_0 u \frac{u-2-\delta}{1+\delta u} + \mathscr{S}_0 u^\gamma \left(\frac{2\sqrt{a}}{\tan(2\psi)}\right)^2, \tag{3.24}$$

where $a = 2(4\mathscr{S}_0 u^\gamma)^3/\pi^2 n$ and $\tan\psi = (\tan\frac{\phi}{2})^{1/3}$ with $\tan\phi = -2\frac{\sqrt{a}}{3}$.

3.4 Nucleonic and Hyperonic matter: FSU2H model

Tolós, Centelles and Ramos [10] started from the Relativistic Mean Field model of matter, where the baryons interact through the exchange of mesons, in order to provide a covariant description of the EoS and nuclear systems.

The Lagrangian density can be expressed as the sum of the baryons (b), leptons (l) and mesons (m) Lagrangian densities:

$$\mathcal{L} = \sum_b \mathcal{L}_b + \mathcal{L}_m + \sum_{l=e,\mu} \mathcal{L}_l, \tag{3.25}$$

with the lepton (electrons and muons) and m the possible exchanged mesons (σ,ω,ρ and ϕ). Their respective Lagrangians are given by

$$\mathcal{L}_b = \bar{\Psi}_b(i\gamma_\mu\partial^\mu - q_b\gamma_\mu A^u - m_b + g_{\sigma b}\sigma - g_{\omega b}\gamma_\mu\omega^\mu - g_{\phi b}\gamma_\mu\phi^\mu - g_{\rho b}\gamma_\mu\vec{I}_b\,\vec{\rho}^{\,\mu})\Psi_b, \tag{3.26}$$

$$\mathcal{L}_l = \bar{\psi}_l\left(i\gamma_\mu\partial^\mu - q_l\gamma_\mu A^\mu - m_l\right)\psi_l, \tag{3.27}$$

$$\begin{aligned}\mathcal{L}_m = {} & \frac{1}{2}\partial_\mu\sigma\partial^\mu\sigma - \frac{1}{2}m_\sigma^2\sigma^2 - \frac{\kappa}{3!}(g_{\sigma N}\sigma)^3 - \frac{\lambda}{4!}(g_{\sigma N}\sigma)^4 - \frac{1}{4}\Omega^{\mu\nu}\Omega_{\mu\nu} + \frac{1}{2}m_\omega^2\omega_\mu\omega^\mu \\ & + \frac{\zeta}{4!}(g_{\omega N}\omega_\mu\omega^\mu)^4 - \frac{1}{4}\vec{R}^{\mu\nu}\vec{R}_{\mu\nu} + \frac{1}{2}m_\rho^2\vec{\rho}_\mu\vec{\rho}^{\,\mu} + \Lambda_\omega g_{\rho N}^2\vec{\rho}_\mu\vec{\rho}^{\,\mu}g_{\omega N}^2\omega_\mu\omega^\mu \\ & - \frac{1}{4}P^{\mu\nu}P_{\mu\nu} + \frac{1}{2}m_\phi^2\phi_\mu\phi^\mu - \frac{1}{4}F^{\mu\nu}F_{\mu\nu},\end{aligned} \tag{3.28}$$

where Ψ_b and Ψ_l are the baryon and lepton Dirac fields, respectively, while the mesonic and electromagnetic field strength tensors are $\Omega_{\mu\nu} = \partial_\mu\omega_\nu - \partial_\nu\omega_\mu$, $\vec{R}_{\mu\nu} = \partial_\mu\vec{\rho}_\nu - \partial_\nu\vec{\rho}_\mu$, $P_{\mu\nu} = \partial_\mu\phi_\nu - \partial_\nu\phi_\mu$ and $F_{\mu\nu} = \partial_\mu A_\nu - \partial_\nu A_\mu$. The meson couplings to a certain baryon are denoted by g (with N indicating nucleon). The electromagnetic couplings are written as q and the baryon, meson and lepton masses by m. The isospin operator is denoted by the vector $\vec{I}_b$.

The Dirac equations for baryons and leptons are presented below in which the effective baryon masses are set to $m_b^* = m_b - g_{\sigma b}\sigma$,

$$\begin{aligned}(i\gamma_\mu\partial^\mu - q_b\gamma_0 A^0 - m_b^* - g_{\omega b}\gamma_0\omega^0 - g_{\phi b}\gamma_0\phi^0 - g_{\rho b}I_{3b}\gamma_0\rho_3^0)\Psi_b = 0, \\ \left(i\gamma_\mu\partial^\mu - q_l\gamma_0 A^0 - m_l\right)\psi_l = 0.\end{aligned} \tag{3.29}$$

Now, following the Euler-Lagrange equations, the equations of motion for the meson fields in the mean-field approximation are expressed in terms of the respective meson mean-field expectation values ($\bar{\sigma} =< \sigma >$, $\bar{\rho} =< \rho_3^0 >$, $\bar{w} =< w^0 >$ and $\bar{\phi} =< \phi^0 >$) as

$$\begin{aligned}& m_\sigma^2\,\bar{\sigma} + \frac{\kappa}{2}g_{\sigma N}^3\bar{\sigma}^2 + \frac{\lambda}{3!}g_{\sigma N}^4\bar{\sigma}^3 = \sum_b g_{\sigma b}n_b^s, \\ & m_\omega^2\,\bar{\omega} + \frac{\zeta}{3!}g_{\omega N}^4\bar{\omega}^3 + 2\Lambda_\omega g_{\rho N}^2\,g_{\omega N}^2\bar{\rho}^2\bar{\omega} = \sum_b g_{\omega b}n_b, \\ & m_\rho^2\,\bar{\rho} + 2\Lambda_\omega g_{\rho N}^2 g_{\omega N}^2\bar{\omega}^2\bar{\rho} = \sum_b g_{\rho b}I_{3b}n_b, \\ & m_\phi^2\bar{\phi} = \sum_b g_{\phi b}n_b\ ,\end{aligned} \tag{3.30}$$

where I_{3b} is the third component of isospin of baryon b with the convention $I_{3p} = +1/2$.

The baryonic and leptonic Fermi energies in terms of their Fermi momenta, k_{Fb} and k_{Fl}, are described by

$$\begin{aligned} E_{Fb} &= \sqrt{k_{Fb}^2 + m_b^{*2}} \ , \\ E_{Fl} &= \sqrt{k_{Fl}^2 + m_l^2} \ , \end{aligned} \tag{3.31}$$

In this way, the scalar and vector densities for baryons b and leptons l look like:

$$\begin{aligned} n_b^s &= \frac{m_b^*}{2\pi^2}\left[E_{Fb}k_{Fb} - m_b^{*2}\ln\frac{k_{Fb}+E_{Fb}}{m_b^*}\right] \ , \\ n_b &= \frac{k_{Fb}^3}{3\pi^2} \ , \\ n_l &= \frac{k_{Fl}^3}{3\pi^2} \ . \end{aligned} \tag{3.32}$$

The energy density of the system is given by

$$\begin{aligned} \varepsilon = &\sum_b \varepsilon_b + \sum_l \varepsilon_l + \frac{1}{2}m_\sigma^2\bar{\sigma}^2 + \frac{1}{2}m_\omega^2\bar{\omega}^2 + \frac{1}{2}m_\rho^2\bar{\rho}^2 + \frac{1}{2}m_\phi^2\bar{\phi}^2 + \frac{\kappa}{3!}(g_\sigma\bar{\sigma})^3 \\ &+ \frac{\lambda}{4!}(g_\sigma\bar{\sigma})^4 + \frac{\zeta}{8}(g_\omega\bar{\omega})^4 + 3\Lambda_\omega(g_\rho g_\omega\bar{\rho}\,\bar{\omega})^2, \end{aligned} \tag{3.33}$$

with the energy densities of baryons and leptons:

$$\begin{aligned} \varepsilon_b &= \frac{1}{8\pi^2}\left[k_{Fb}E_{Fb}^3 + k_{Fb}^3E_{Fb} - m_b^{*4}\ln\frac{k_{Fb}+E_{Fb}}{m_b^*}\right], \\ \varepsilon_l &= \frac{1}{8\pi^2}\left[k_{Fl}E_{Fl}^3 + k_{Fl}^3E_{Fl} - m_l^4\ln\frac{k_{Fl}+E_{Fl}}{m_l}\right]. \end{aligned} \tag{3.34}$$

The pressure of the system is computed using the thermodynamic relation

$$P = \sum_i \mu_i n_i - \varepsilon, \tag{3.35}$$

with the baryonic and leptonic chemical potentials given by

$$\mu_b = E_{Fb} + g_{\omega b}\,\bar{\omega} + g_{\rho b}\,I_{3b}\,\bar{\rho} + g_{\phi b}\,\bar{\phi}\ ,$$
$$\mu_l = E_{Fl}. \tag{3.36}$$

In this context, the parameters of the EoS are fitted with a view to fulfil the saturation properties of nuclear matter and finite nuclei, constraints of the high-density nuclear pressure from heavy-ion collisions and the $2M_\odot$ observations, while keeping small stellar radius in line with certain analysis [6]. The parameters are shown in the Table 3.1.

$\boldsymbol{m_\sigma}$ (MeV)	497.479
$\boldsymbol{m_w}$ (MeV)	782.500
$\boldsymbol{m_\rho}$ (MeV)	763.000
$\boldsymbol{g^2_{\sigma N}}$	102.7200
$\boldsymbol{g^2_{wN}}$	169.5315
$\boldsymbol{g^2_{\rho N}}$	197.2692
$\boldsymbol{\kappa}$	4.0014
$\boldsymbol{\lambda}$	-0.013298
$\boldsymbol{\xi}$	0.008
$\boldsymbol{\Lambda_w}$	0.045

Table 3.1: Parameters of the FSU2H model from [10]. The mass of the nucleon is m_N=939 MeV.

In brief, the parametrization of FSU2H model leads to obtain the following properties at saturation density (n_0=0.1505 fm^{-3}). The energy per particle results in E/A=-16.28 MeV, the compressibility is K=238.0 MeV and the effective nucleon mass in symmetric nuclear matter leads to m^*_N/m_N=0.593. The symmetry energy is set to E_{sym}=30.5 MeV whose slope and curvature are defined by L=44.5 and K_{sym}=86.7 MeV, respectively. Finally, the pressure of pure neutron matter is P_{PNM}=2.30 MeV fm^{-3} at n_0.

As the interior of neutron stars stays globally neutral and in conditions of β-equilibrium [Eqs. (3.1) & (3.2)], therefore, the chemical potentials and the number densities of each particle in a neutron star are related to the beta-conditions already explained [see Eqs. (3.10) & (3.11)].

Finally, solving the Dirac equations (3.29) for the baryons and leptons with the mesonic field equations (3.30) for a given total baryon density n and obtaining the corresponding chemical potential from each species, one can determine the energy density and pressure of the β-stable neutron star as functions of density.

3.5 Equations of state

In this section, we are going to represent the EoSs for the H&H and FSU2H models employed in this study, in order to analyse them and distinguish their characteristics. Indeed, Figures 3.1 and 3.2 show the energy density and pressure of the system, respectively, as functions of the baryon density for the H&H and FSU2H models.

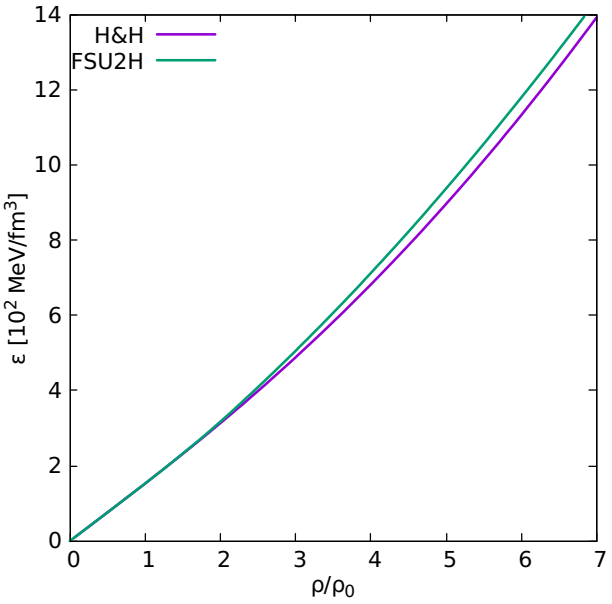

Figure 3.1: Energy density vs. baryon density for the different models presented in the text: H&H (Heiselberg & Hjorth-Jensen [11]) and FSU2H (Tolós, Centelles & Ramos [10]).

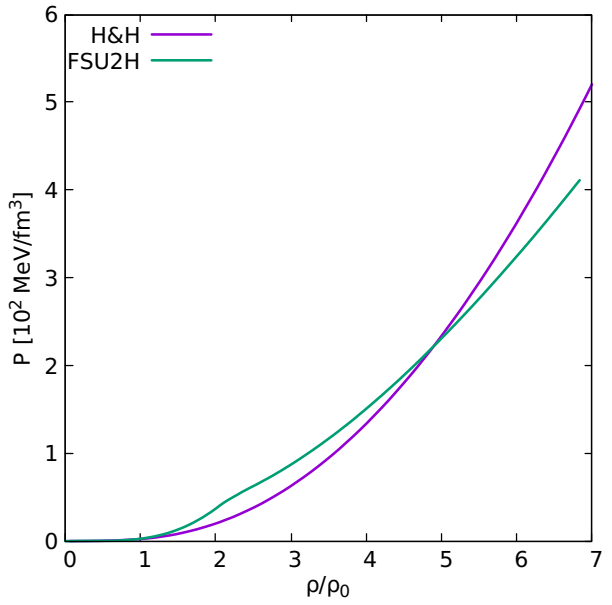

Figure 3.2: Pressure vs. baryon density for the different models presented in the text: H&H (Heiselberg & Hjorth-Jensen [11]) and FSU2H (Tolós, Centelles & Ramos [10]).

On the one hand, from Figure 3.2, one can extract some conclusions. The FSU2H model has a stiffer behaviour in the range $n_0 \leq n \leq 5n_0$ than the H&H model, although the appearance of hyperons ($\sim 2n_0$) softens the pressure of the FSU2H system so that the H&H EoS becomes stiffer from $\simeq 5n_0$ onwards.

The change in the pressure conduct due to the introduction of hyperons can be explained in terms of the Fermi pressure, which reduces with the presence of this new species that starts to fill up its own Fermi sea. For that reason, the H&H model gives a harder EoS for larger densities. The lack of new species prevents the reduction of the pressure and the electrons, protons and neutrons continue occupying higher energy states of their own Fermi seas, rising the pressure of the neutron star.

In this context, greater pressure values mean having a system harder to compress and, accordingly, it is able to resist more against gravity. In fact, a stronger bearing at saturation densities is translated into larger neutron star radii and a stiffer conduct at suprasaturation densities is marked by higher masses.

On the other hand, the FSU2H energy density in function of the baryon density is larger than the H&H EoS in all the density range explored in Figure 3.1.

Finally, Figure 3.3 represents the dependence of the pressure on the energy density for both models in study. As expected this plot shows the same behaviour sustained by Fig. 3.2 as both pressure and energy density increase monotonically with density. We show Figure 3.3 because pressure and energy density enter in the structure equations of neutron stars, presented in the next chapter.

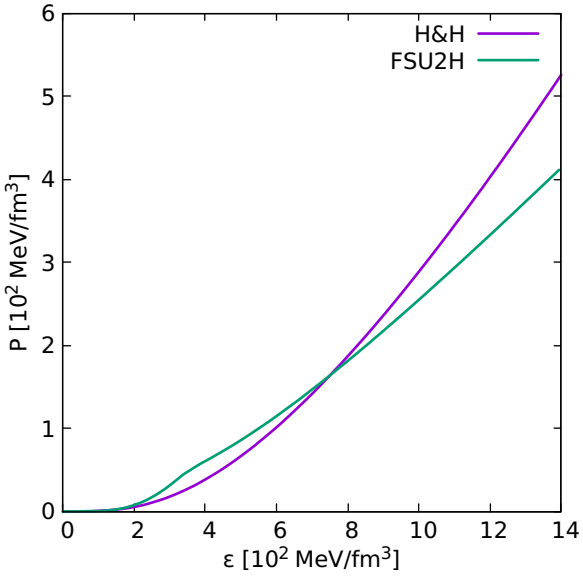

Figure 3.3: Pressure vs. energy density for the different models presented in the text: H&H (Heiselberg & Hjorth-Jensen [11]) and FSU2H (Tolós, Centelles & Ramos [10]).

Chapter 4

Non-rotating neutron stars: TOV equations

In order to determine the structure of a neutron star, Einstein's General Relativity Theory is needed as we are dealing with one of the densest objects in the Universe. For this reason, the equations that describe a non-rotating star in equilibrium (or Schwarzschild star) start from Einstein's field equations. Using Gravitational Units (G=c=1)[i], the Einstein's field equations are given by

$$G^{\mu\nu} = -8\pi T^{\mu\nu}, \tag{4.1}$$

where $G^{\mu\nu}$ is the so-called Einstein tensor and $T^{\mu\nu}$ is the energy-momentum tensor.

The solution of the Einstein's equations for a static, spherically symmetric and relativistic star are known as the Tolman-Oppenheimer-Volkoff equations (TOV equations) [14, 15]. For a given EoS, and a given value of the central density, the stellar structure equations of hydrostatic equilibrium in General Relativity are:

$$\frac{dp(r)}{dr} = -\frac{(\varepsilon(r) + p(r))(M(r) + 4\pi r^3 p(r))}{r(r - 2M(r))} \tag{4.2}$$

and

$$\frac{dM(r)}{dr} = 4\pi r^2 \varepsilon(r). \tag{4.3}$$

By re-writing Equation (4.2), we arrive to

$$\frac{dp(r)}{dr} = -\frac{M(r)\varepsilon(r)}{r^2} \frac{\left(1 + \frac{p(r)}{\varepsilon(r)}\right)\left(1 + \frac{4\pi r^3 p(r)}{M(r)}\right)}{\left(1 - \frac{2M(r)}{r}\right)}. \tag{4.4}$$

[i] We are going to use Gravitational Units from now to the end of this project.

The equation can be interpreted as follows [1]. On the one hand, the left-hand side of Eq. (4.4) is the net force acting outward on the surface of the shell by the pressure difference $dp(r)$. On the other hand, the first factor of the right-hand side of Eq. (4.4) is the attractive gravity Newtonian force acting on the shell by the mass enclosed. The second factor on the right-hand side of the equation refers to the corrections from General Relativity. Thus, these equations express the balance at each r between the internal pressure and the gravitational attraction of the mass enclosed at r.

Moreover, the integration of the pressure $p(r)$ and the enclosed mass to a given radius, $M(r)$, must be performed outward; starting at the star's centre (r=0) where the mass of the star is M=0 and the pressure is p_C. We finish when the pressure becomes $p = 0$, which defines the edge of the star. The point at which the pressure vanishes defines the radius of a non-rotating star, R.

The integration of equation (4.3) from the centre of the star up to its radius defines its gravitational mass:

$$M_G = 4\pi \int_0^R dr r^2 \varepsilon(r). \tag{4.5}$$

Chapter 5

Rotating neutron stars: Hartle-Thorne approach

When the core of a massive star collapses to produce a neutron star, conservation of angular momentum assures its enhanced rotation. That rotation necessarily breaks spherical symmetry as the rotating star is centrifugally deformed, only maintaining its axial symmetry. The relevance of the deformation depends on the angular velocity Ω of the star: the quicker, the flatter. Therefore, in this chapter we are interested in effects of rotation on the internal structure of relativistic stars.

However, this symmetry breaking holds some difficulties when constructing the structure equations of rotating neutron stars in comparison with the non-rotating case. The main issues are related to the deformation of the star, the increase of its mass due to rotation and the consequent alteration of the geometry of space-time, and the general relativistic effect of the dragging of local inertial frames (Lense-Thirring effect [12]).

The angular velocity associated with dragging of local inertial frames is fundamental to rotation in General Relativity, carrying its name because of its effect. For example, imagine a particle dropped from rest at a great distance from a star. If the star was not rotating, the particle would fall directly toward the centre of that star. But if the star was rotating, the particle would experience an increasing drag in the direction of rotation of the star as it approaches [12]. See Figure 5.1.

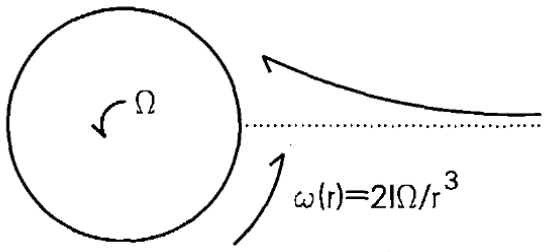

Figure 5.1: Schematic of the trajectory of a particle dropped from infinity to a rotating star. Image from [12].

The so-called frame-dragging frequency is largest at the centre of a rotating star and falls to cero at large distances where spacetime becomes flat. Therefore, the rotation of local inertial frames has a true effect on the internal structure of rotating stars.

Indeed, if we could behave as an observer in an inertial frame near a rotating star, we would rotate around our centre relative to the distant stars, rotating the more rapidly, the closer we approach the star. Hence, we would need a rocket or other ways of propulsion to stop our own rotation.

In order to determine the properties of rotating neutron stars, we will present the set of equations that we have used coming from the perturbative method developed by Hartle and Thorne ([31], [32]). For years, this method was thought to be valid only for slowly rotating stars. However nowadays, it is known to be valid up to the Keplerian frequency, which is the frequency at which a rotating star would shed matter at its equator, within a few percent of the exact numerical solution determined by a direct numerical integration of Einstein's equations [33].

In summary, we are interested in obtaining the properties of neutron stars, such as the mass, moment of inertia and angular momentum of rotating neutron stars.

5.1 Hartle-Thorne approach

In equilibrium, a rotating star attains a balance between pressure, gravitational and centrifugal forces. As it has already mentioned, the structure of a rotating star depends on its frequency due to the rotation of the local inertial frames. Then, the centrifugal force acting on a fluid element of the star depends on the difference between the total angular frequency of the star Ω and the frequency $w(r)$ of the local inertial frame at the location (r, θ) of the fluid element as

$$\bar{w}(r) \equiv \Omega - w(r), \tag{5.1}$$

being $\bar{w}(r)$ the relative angular velocity.

Hartle in Ref. [31] quoted the following differential equation where it is shown that $\bar{w}(r)$ depends only on the radial coordinate r to lowest order in Ω:

$$\frac{1}{r^4}\frac{d}{dr}\left(r^4 j(r)\frac{d\bar{w}(r)}{dr}\right) + \frac{4}{r}\frac{dj(r)}{dr}\bar{w}(r) = 0. \tag{5.2}$$

At the centre of the star, the magnitude $\bar{w}(r)$ is subjected to the boundary conditions $\bar{w}(0) = \bar{w}_c$ and $(d\bar{w}(r)/dr)_{r=0} = 0$, with $\bar{w}_c$ being an arbitrary constant value.

The function $j(r)$ is defined in terms of the metric for a Schwarzchild star as

$$j(r) \equiv e^{-\nu(r)}\sqrt{1-\frac{2M(r)}{r}}, \quad r < R, \tag{5.3}$$

$$j(r) \equiv 1, \quad r \geq R. \tag{5.4}$$

The metric function $\nu(r)$ fulfils the equation

$$\frac{d\nu(r)}{dr} = \frac{M(r) + 4\pi r^3 p(r)}{r(r-2M(r))}, \tag{5.5}$$

with $M(r)$ and $p(r)$ being the solutions of the TOV equations.

The former differential equation solution must match the exterior solution which can be deduced from Eqs. (5.3) and (5.4) and reads as

$$e^{-\nu(r)} = \left(1-\frac{2M(r)}{r}\right)^{-1/2}, \quad r \geq R. \tag{5.6}$$

If $\nu(r)$ is a solution for Eq. (5.5), adding any constant to that solution of $\nu(r)$, we still have a valid solution. So, we obtain the correct condition at the surface of the star R if we make the change:

$$\nu(r) \to \nu(r) - \nu(R) + \frac{1}{2}\ln\left(1-\frac{2M}{R}\right), \quad r \leq R. \tag{5.7}$$

Now, Equation (5.1) was defined inside of the star but outside the star one has to accomplish the following relation. Thus, the relative angular velocity when one reaches the surface is given by

$$\bar{w}(r) = \Omega - \frac{2}{r^3}J(\Omega) \quad r \geq R, \tag{5.8}$$

where $J(\Omega)$ is the total angular momentum of the star given by:

$$J(\Omega) = \frac{8\pi}{3}\int_0^R dr r^4 \frac{p(r)+\varepsilon(r)}{\sqrt{1-\frac{2M(r)}{r}}}(\Omega - w(r))e^{-\nu(r)}. \tag{5.9}$$

From the total angular momentum of the star, we are able to define the moment of inertia of the star as:

$$I \equiv \frac{J(\Omega)}{\Omega}. \tag{5.10}$$

Thus, it is important keep in mind the relativistic corrections added to the moment of inertia of the star coming from Eq. (5.9). Those corrections are due to the dragging of local inertial frames that is $\bar{w}(r)/\Omega < 1$, the red-shift ($e^{-\nu(r)}$) and space curvature ($1/\sqrt{1-\frac{2M(r)}{r}}$) factors.

Moreover, we may notice that, outside the star, the angular velocity of the local inertial frame can be written using equations (5.8) and (5.10) as:

$$w(r) = \frac{2J(\Omega)}{r^3} = \frac{2I}{r^3}\Omega, \quad r \geq R. \tag{5.11}$$

This last expression together with Equation (5.2) permits us to calculate the dragging angular velocity everywhere by taking into account that w vanishes far away from the star. Consequently, by matching both relations, it may be noticed that $\bar{w}(r)/\Omega$ is a universal function for a given EoS and value of the central density [12], so that:

$$\frac{w(r)}{\Omega} = \frac{w'(r)}{\Omega'}. \tag{5.12}$$

This relation is proved in Figure 5.2, which shows that for a given EoS and value of the central density (meaning, a given star with a mass and radius), the ratio of the frame-dragging frequency to the star frequency is a universal function.

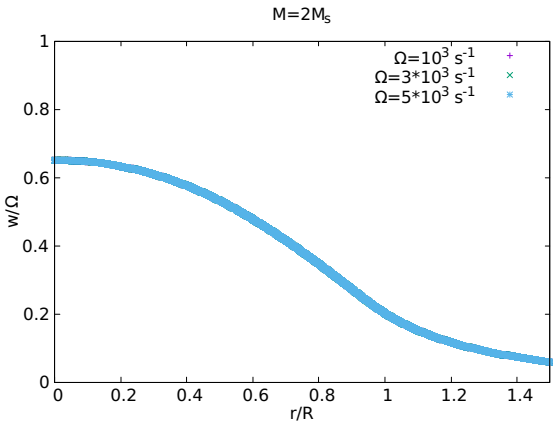

Figure 5.2: Ratio of frame-dragging angular velocity to three different angular velocities for the maximum mass star of the FSU2H EoS.

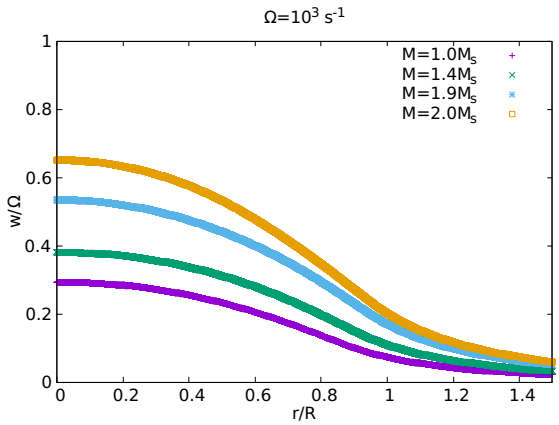

Figure 5.3: Ratio of the frame-dragging angular velocity to the angular velocity for four members of a stellar sequence of the FSU2H EoS.

In Figure 5.3, it is also shown the ratio between the frame-dragging angular velocity with an angular velocity of Ω=1000 s^{-1} but for four different members of the stellar sequence given by the FSU2H EoS, among them the minimum and maximum mass stars. Then, the relation is always less than unity and decreases monotonically with r. Furthermore, the value of this ratio increases with the mass of the star. Consequently, we appreciate bigger effects of the relative angular velocity for stars that have higher central densities.

Now, as we have already deduced the expressions due to rotation and explained some necessary details related to it, we are able to calculate the deformations of the star due to the rotation. So, the increase in mass of a star with central energy density ε_c and angular velocity Ω can be obtained from the relation

$$\Delta M(\Omega) = m_0(R) + \frac{J(\Omega)^2}{R^3}. \tag{5.13}$$

In this expression, R is the spherical radius from the non-rotating star and the function $m_0(r)$ is the monopole mass perturbation that can be determined by integrating the equation

$$\begin{aligned}\frac{dm_0(r)}{dr} =& 4\pi r^2 \frac{d\varepsilon}{dp}(\varepsilon(r)+p(r))p_0(r) + \frac{1}{12}j(r)^2 r^4 \left(\frac{d\bar{w}(r)}{dr}\right)^2 \\ &+ \frac{8\pi}{3} r^5 j(r)^2 \frac{\varepsilon(r)+p(r)}{r-2M(r)}\bar{w}(r)^2.\end{aligned} \tag{5.14}$$

This integration has to be done simultaneously with that for the monopole pressure perturbation $p_0(r)$ function given by:

$$\begin{aligned}\frac{dp_0(r)}{dr} =& -\frac{1+8\pi r^2 p(r)}{(r-2M(r))^2} m_0(r) - 4\pi \frac{(\varepsilon(r)+p(r))r^2}{r-2M(r)} p_0(r) \\ &+ \frac{1}{12}\frac{r^4 j(r)^2}{r-2M(r)}\left(\frac{d\bar{w}(r)}{dr}\right)^2 + \frac{1}{3}\frac{d}{dr}\left(\frac{r^3 j(r)^2 \bar{w}(r)^2}{r-2M(r)}\right),\end{aligned} \tag{5.15}$$

with the boundary conditions $m_0(0)= p_0(0)=0$. With these boundary conditions, the rotating star will have the same central density as the non-rotating one.

Finally, the deformation of the star due to the rotation can be characterised by the eccentricity, which describes the shape of the star at its surface. It is defined as

$$e = \sqrt{1 - \left(\frac{R_p}{R_{eq}}\right)^2}, \tag{5.16}$$

where R_p and R_{eq} are the polar and equatorial radii of the rotational deformed star, respectively. In the Hartle-Thorne approach, the equatorial and polar radii are obtained from the radius R in the non-rotating star configuration and the consequent displacements in the rotating configuration:

$$\begin{aligned} R_{eq} &\approx R + \xi_0(R) - \frac{1}{2}\xi_2(R), \\ R_p &\approx R + \xi_0(R) + \xi_2(R). \end{aligned} \tag{5.17}$$

The quantities $\xi_0(r)$ and $\xi_2(r)$ are referred to the spherical and quadrupole stretching functions:

$$\begin{aligned} \xi_0(r) &= -p_0(r)(\varepsilon(r) + p(r)) \left(\frac{dp(r)}{dr}\right)^{-1}, \\ \xi_2(r) &= -p_2(r)(\varepsilon(r) + p(r)) \left(\frac{dp(r)}{dr}\right)^{-1}. \end{aligned} \tag{5.18}$$

As we can see, they are defined in terms of the energy density $\varepsilon(r)$, pressure density (r), monopole pressure perturbation $p_0(r)$ and the quadrupole pressure perturbation $p_2(r)$, which is given by

$$p_2(r) = -h_2(r) - \frac{1}{3}(r\bar{w}(r))^2 e^{-2\nu(r)}. \tag{5.19}$$

The function $h_2(r)$, which appears in the previous equation, is the solution of the following equation

$$\begin{aligned} \frac{dh_2(r)}{dr} = &\left(-2\frac{d\nu(r)}{dr} + \frac{2r}{r-2M(r)}\left(\frac{d\nu(r)}{dr}\right)^{-1}\left(2\pi(\varepsilon(r)+p(r)) - \frac{M(r)}{r^3}\right)\right) h_2(r) \\ &- \frac{2}{r(r-2M(r))}\left(\frac{d\nu(r)}{dr}\right)^{-1} v_2(r) \\ &+ \frac{1}{6}\left(r\frac{d\nu(r)}{dr} - \frac{1}{2(r-2M(r))}\left(\frac{d\nu(r)}{dr}\right)^{-1}\right) r^3 j(r)^2 \left(\frac{d\bar{w}(r)}{dr}\right)^2 \\ &- \frac{1}{3}\left(r\frac{d\nu(r)}{dr} + \frac{1}{2(r-2M(r))}\right)\left(\frac{d\nu(r)}{dr}\right)^{-1} (r\bar{w}(r))^2 \frac{dj(r)^2}{dr}. \end{aligned} \tag{5.20}$$

It must be simultaneously integrated together with the following equation

$$\frac{dv_2(r)}{dr} = -2\frac{d\nu(r)}{dr}h_2(r) + \left(\frac{1}{r} + \frac{d\nu(r)}{dr}\right)\left(-\frac{r^3}{3}\frac{dj(r)^2}{dr}\bar{w}(r)^2 + \frac{j(r)^2}{6}r^4\left(\frac{d\bar{w}(r)}{dr}\right)^2\right), \quad (5.21)$$

with boundary conditions $v_2(0)$=$h_2(0)$=0 and $v_2(\infty)$=$h_2(\infty)$=0.

To sum up, we have shown all necessary expressions that determining the structure of a rotating neutron star.

5.2 Numerical calculation

In this section, we explain how to deal with the equations that permit us to determine the deformation of rotating neutron stars. We have developed a Fortran programme within the Hartle-Thorne approach that is shown in Appendix A.1.

First of all, we read our data from the EoS and solve the TOV equations [Eqs. (4.2) & (4.3)] in order to know the gravitational mass and radius for the static solution. We start the integration from the origin having as initial conditions M(0)=0 and a particular value of the central pressure $p(0) = p_c$, until it becomes zero with R the radius of the star and $M(R)$ its gravitational mass.

The integration of the metric function $\nu(r)$ [Eq. (5.5)] is done together with the TOV equations, selecting the convenient value of $\nu(0) = 0$. As it is figured out, since $M(r)$ and $p(r)$ are the variables of the TOV equations, one can obtain $\nu(r)$ simultaneously.

Once we have the result for the metric function $\nu(r)$, we find the correct condition of the metric function at R by applying Eq. (5.7). We also work out the j(r) function [Eq. (5.3)] and the relative dragging frequency [Eq. (5.2)], being the arbitrary constant value fixed to $\bar{w}_c = 1$ for convenience in order to accomplish the boundary conditions, and, finally, the total angular momentum [Eq. (5.9)].

Now, using Equation (5.8), we are able to find the value for the total angular velocity of the star, named as Ω_{arb}. As we are interested to chose the total angular momentum of the star Ω, one must scale the relative angular velocity $\bar{w}(r)$ as

$$\bar{w}_{const} = \frac{\Omega}{\Omega_{arb}}. \quad (5.22)$$

Consequently, one should apply the rescale not only to the relative angular velocity but also to the respective derivative and total angular momentum of the star.

Furthermore, we are able to calculate the moment of inertia [Eq. (5.10)] and the Keplerian frequency Ω_K. We use the approximation [12]

$$\Omega_K = 0.65 \left(\frac{M}{R^3}\right)^{1/2}. \tag{5.23}$$

Next, we begin the integration for the monopole mass [Eq. (5.14)], the monopole pressure [Eq. (5.15)], the h_2 function [Eq. (5.20)] and v_2 function [Eq. (5.21)] with the respective boundary conditions already mentioned. Once the integration has finished, we are able to get the increment of mass due to rotation given in Eq. (5.13).

Lastly, we can do the integration for the quadrupole pressure [Eq. (5.19)] and the stretching functions [Eq. (5.18)], which allow us getting the polar and equatorial radii [Eq. (5.17)] and the star eccentricity [Eq. (5.16)].

All these steps are repeated for every star, that means for every central density given in the EoS data file.

Chapter 6

Results

In this chapter, we are going to show the results obtained after solving the TOV equations for non-rotating neutron stars and, afterwards, the ones obtained after applying the Hartle-Thorne approach of rotating neutron stars, which is the main interest of this project. The results for rotating neutron stars will be classified according to the deformation in size and mass due to rotation and, the moment of inertia associated to those rotating neutron stars.

The calculations have been performed for the nucleonic H&H and the hyperonic FSU2H EoSs, for different rotating velocities (Ω=1000, 3000 & 5000 Hz). Those values have been chosen taking into account that pulsars rotating with periods bigger than 700 Hz ($\sim$ 4500 s^{-1}) have not been observed yet, despite the fact that it does not exist an upper limit banning a more rapid rotation.

Therefore, we will compare the results of the two models for the selected rotating velocities and try to understand their differences.

6.1 Non-rotating neutron stars

First of all, it is important to understand the features of non-rotating neutron stars. For that reason, in Figure 6.1, we show the mass and radius relation obtained for both EoSs after solving the TOV equations (eqs. (4.2) & (4.3)).

For stars with approximately the same mass, we denote a substantial difference between their radii. The FSU2H model gives rise to the larger radii as compared to the H&H EoS, a fact that is related to its stiffness (see Table 6.1). Even though, both EoSs give radii within the estimated range (10.7-13.1 km).

Consequently, it turns out that only the FSU2H model achieves the maximum mass limit of $2M_\odot$ given by observations. The maximum non-rotating neutron star masses are found to be of $1.94M_\odot$ for H&H EoS and $2.02M_\odot$ for FSU2H model, with the corresponding radii of R=10.21 km and R=12.13 km, as seen in Table 6.1.

In brief, a stiffer EoS leads to larger masses but also bigger stellar radii.

	$\mathbf{M/M_\odot}$	$\mathbf{R}$ (km)	$\boldsymbol{\rho_c}$ (fm^{-3})	$\boldsymbol{\varepsilon_c}$ (MeV/fm^3)	$\boldsymbol{\Omega_k}(s^{-1})$
H&H	1.04	12.06	0.40	400	5773
	1.40	11.91	0.52	537	6815
	1.90	10.77	0.97	1153	9239
	1.94	10.21	1.21	1555	10092
FSU2H	1.02	13.04	0.28	276	5088
	1.39	13.29	0.33	327	5761
	1.90	13.14	0.53	573	6843
	2.02	12.13	0.87	1040	7971

Table 6.1: Mass (M) and radius (R) obtained for H&H and FSU2H models, together with the corresponding central density and energy density. The Keplerian frequency is also shown for each case.

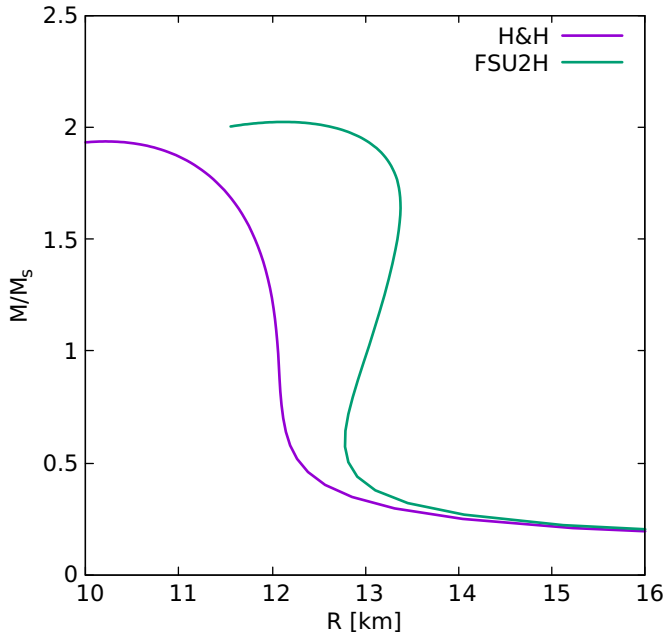

Figure 6.1: Plot of the mass and radius relation for the FSU2H and H&H EoSs for non-rotating neutron stars.

6.2 Rotating neutron stars

Before starting the analysing of the rotating neutron stars results, it is of great utility to understand first the relation of our non-rotating neutron stars parameters with the Keplerian frequency.

The Keplerian frequency indicates the upper limit on the rotation of stable neutron stars. Therefore, calculating the Keplerian frequency of a star of mass M and radius R will establish the maximum angular velocity that is capable to support before becoming unstable. Thus, the Keplerian frequency informs us about the angular velocities that our neutron stars can hold up in the rotation.

Figure 6.2 illustrates the dependence of the Keplerian angular velocity Ω_K on the gravitational neutron star mass [Eq. (5.23)], and consequently, on the underlying EoS also. The Keplerian frequency values increase as the gravitational mass of the stellar sequence does.

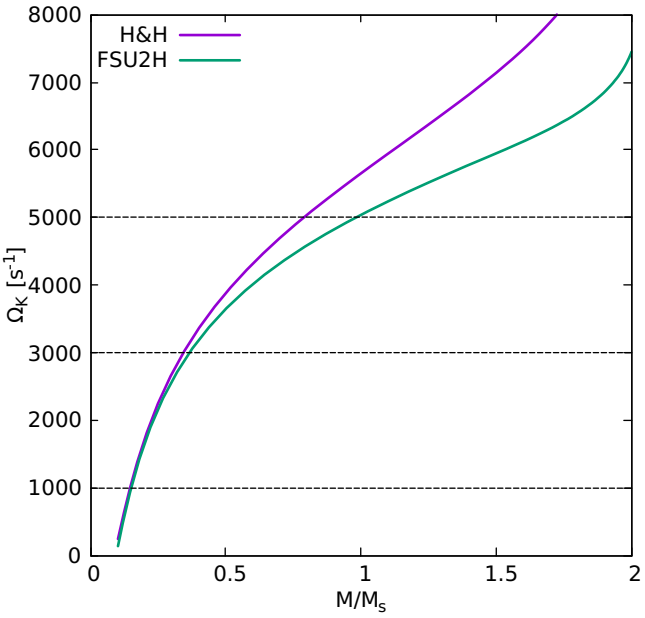

Figure 6.2: Keplerian angular velocity vs gravitational mass of non-rotating neutron stars for different EoSs.

Referring to the EoSs in study, we oserve that the two different models have led to quite different values for Ω_K as a function of M. This difference highlights with the rise of the gravitational mass.

According to Glendenning [12], the dependence of P on ε (Fig. 3.3) has an important impact on the Keplerian frequency. The EoS must be soft at low and intermediate densities and hard at high densities for a neutron star to withstand fast rotation. Such behaviour agrees with the nucleonic H&H model.

Consequently, the largest values for $\Omega_K(M)$ result from the H&H EoS; the reason of its behaviour lies in the smaller values of the star radius that this model produces. Thus, the H&H model will allow higher rotational frequencies for a given mass value.

Lastly, the three horizontal dashed lines represent the three angular velocities that will be employed in our calculations of rotating neutron stars (Ω=1000, 3000, 5000 s^{-1}), setting a limit on the neutron stars that have smaller Keplerian frequency value. Therefore, the neutron stars with Keplerian angular velocities Ω_K below these limiting lines will not be taken into account in the following, as they have arrived at their critical equatorial velocity at which mass-shedding sets in.

6.2.1 Deformation

Firstly, we represent the dependence of the equatorial radius (R_{eq}) with the central energy density for different angular velocities, together with the non-rotating case, for both models in study. Figures 6.3 and 6.4 represent the results obtained with the H&H and FSU2H EoSs, respectively.

For the non-rotating case, the relation of the radius with the central energy density gives us an idea about the compactness of the star. Not only the increase of the central energy density is linked with a decrease of the radius but also with bigger gravitational masses. In consequence, the size of the star is reduced with increasing central energy densities, leading to more compact neutron stars.

Comparing the results of the H&H model with those of the FSU2H one for the same radius, we see that the nucleonic EoS gives a smaller central energy density and gravitational mass, outcoming into more diluted neutron stars than the FSU2H ones.

Moreover, the FSU2H model shows a "wiggle" for $\varepsilon \sim$ 2-4·10^2 MeV/fm^3 which indicates that the same radius is obtained for different central energy densities, meaning different mass configurations and, on consequence, distinct stars. This is clearly seen in Figure 6.1, where the mass-radius plot for non-rotating neutron stars is shown.

Once stars rotate, stars with the same central energy density but rotating faster become more extended due to the equatorial radius growth. Moreover, the deformation of the star is more evident for those stars with lower central energy densities, that is, more diluted stars.

Lastly, comparing both studied models, we observe that FSU2H gives rise to larger equatorial radii values due to its harder EoS for densities around saturation, as previously discussed.

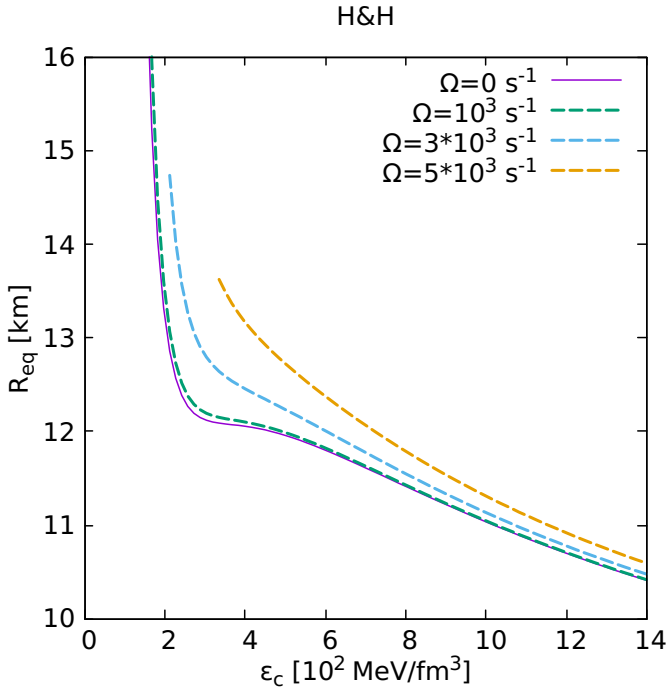

Figure 6.3: Equatorial radius vs. central energy density for different angular frequencies Ω for the H&H EoS.

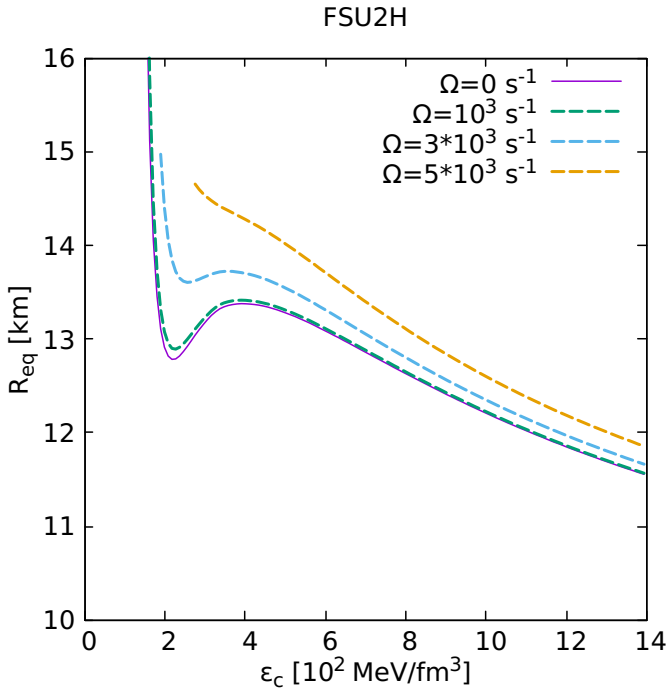

Figure 6.4: Equatorial radius vs. central energy density for different angular frequencies Ω for the FSU2H EoS.

The deformation of the star from its spherical form due to rotation can be also shown by plotting the relation between the polar and equatorial radii. Figures 6.5 and 6.6 show this relation for the nucleonic H&H and the hyperonic FSU2H models, respectively, for different angular velocities.

In accord with the previous conclusions for Figures 6.3 & 6.4, the higher the value of the equatorial radius, the more deviation of the star from its spherical shape. Thus, stars with smaller gravitational masses and, on consequence, bigger non-rotating radii (lower values of ε_c) suffer larger deformations on their aspect than the more massive stars.

Moreover, the deviation from the spherical configuration increases as the angular velocity does, meaning having more oblate neutron stars for faster rotating configurations.

By comparing the results for both models, the representation of polar and equatorial radii seems to give a more extensive deformed aspect for the star configurations of the FSU2H EoS, in concordance with the last conclusions of Figures 6.3 and 6.4. This behaviour will be illustrated more clearly by the observables represented in the following Figures 6.7 and 6.8.

Notice that the number of stars decreases with the implementation of higher rotation. This is due to the fact that the ending point on the right of each angular velocity function is the last star which fulfils the Keplerian condition, and the higher the rotation, the faster this limit of instability is reached.

Finally, in Figures 6.7 and 6.8, we show the eccentricity as a function of the rotational mass for the different angular velocities and both EoSs. This observable also illustrates the deformation of the star due to rotation but by the description of the star's surface [Eq. (5.16)].

For a fixed frequency, the deformation is larger (higher eccentricity) for the less massive stars as this systems are characterised by a smaller Keplerian frequency. Thus, the less massive stars have a larger size (bigger radii and lower central energy density) because they are rotating closer to their mass-shedding limit. Consequently, those systems are more deformed from their original non-rotating spherical configuration.

With the growth of the angular velocity Ω, the eccentricity increases its value approaching unity, which is in agreement with the rise of the degree of deformation of the equatorial and polar radii. In brief, the deformation increases as the system is getting closer to its Keplerian frequency.

Now, by comparing both figures, since the FSU2H model is characterised by smaller Keplerian frequencies, it suffers larger deformations due to rotation than the H&H, thereby showing higher eccentricity values. This behaviour is also supported by our previous discussion of deformation.

Note that eccentricity values very close to unity are not obtained as those values would come from rotating stars with frequencies above the Keplerian limit, and hence, unstable.

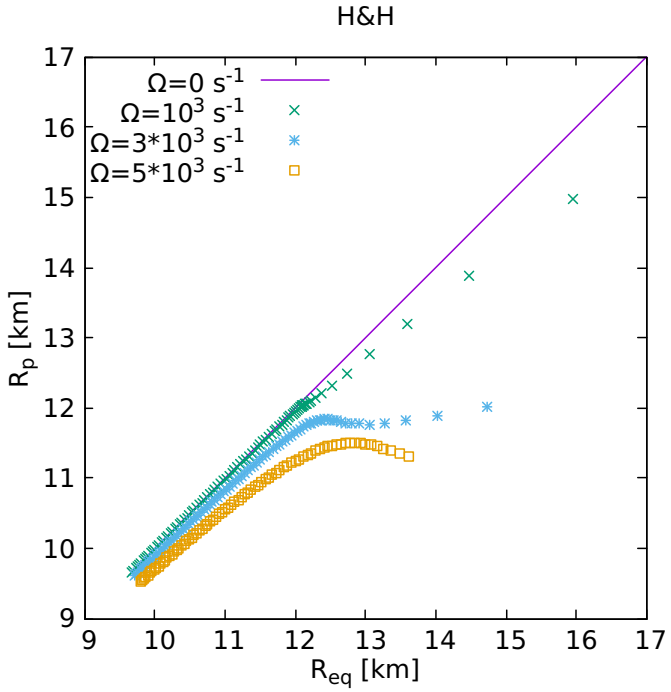

Figure 6.5: Polar vs. equatorial radius for different angular frequencies Ω for the H&H EoS.

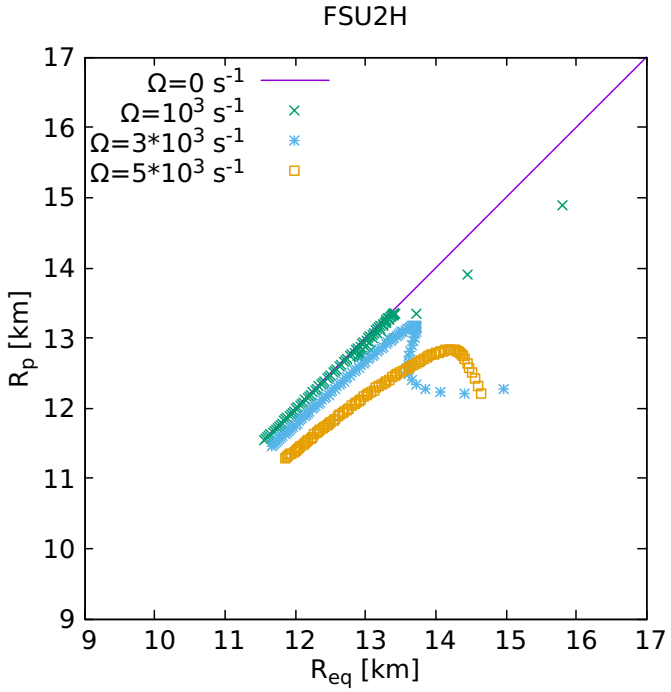

Figure 6.6: Polar vs. equatorial radius for different angular frequencies Ω for the FSU2H EoS.

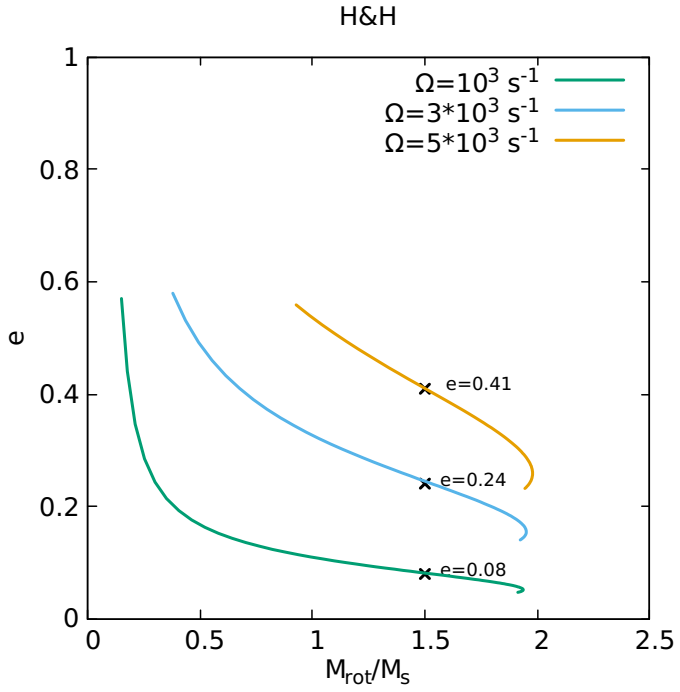

Figure 6.7: Eccentricity vs. rotational mass for different angular frequencies Ω for the H&H EoS.

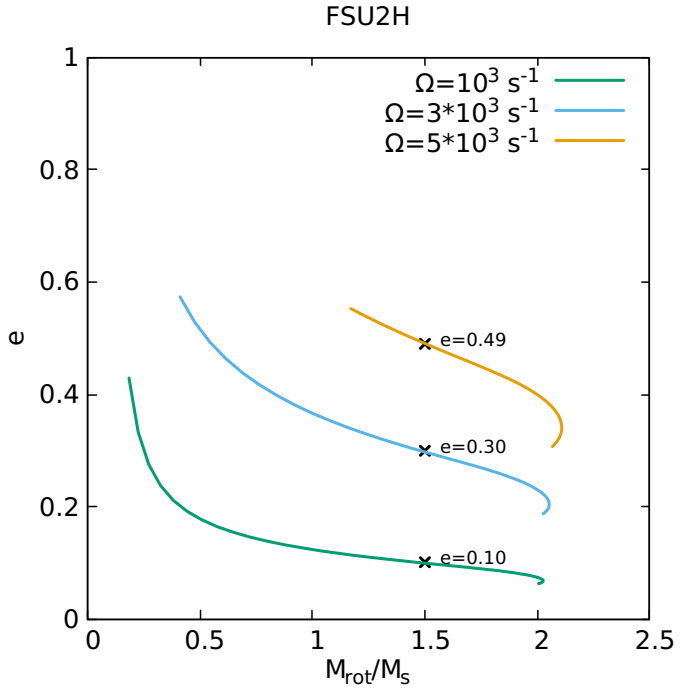

Figure 6.8: Eccentricity vs. rotational mass for different angular frequencies Ω for the FSU2H EoS.

6.2.2 Mass

Firstly, Figures 6.9 and 6.10 display the rotational neutron star mass as a function of central energy density for the H&H and FSU2H models, respectively. Figures 6.11 and 6.12 show the relation between the rotational mass and the non-rotating radius, for the same two models. Plots are represented for the non-rotating as well as the rotating configurations.

In these figures, we observe that the difference between the gravitational and the rotational masses increases with the angular velocity. This can be understood by the fact that the increment of mass due to rotation having a direct dependence with the angular velocity via the total angular momentum of the star as given in Eq. (5.13). In fact, the increase of the angular velocity leads to the increase of the centrifugal force that needs to be compensated by a larger mass.

We remind that the FSU2H EoS is harder than the H&H model, leading to higher gravitational masses and radii as already mentioned. Because of that, the FSU2H model gives rise to larger total angular momentum values, leading to higher increments of mass and bigger rotational masses. We will appreciate more clearly the last argument in Figures 6.15 and 6.16, where the moment of inertia is shown for both EoSs.

In order to finish the analysis of the increment of mass due to rotation, we show the rotational mass as a function of the equatorial radius. The resulting $M-R$ relation for rotating neutron stars is presented for the different angular velocities in Figures 6.13 and 6.14 in case of the H&H and FSU2H EoSs, respectively.

We observe that, for a fixed value of the angular velocity Ω, the increment of the equatorial radius is more relevant for less massive stars, meaning smaller central energy density values. Moreover, the growth on the equatorial radii rises for faster rotations, evidently. Qualitatively, the nucleonic H&H and hyperonic FSU2H models show similar behaviour referring to its shape and increment of mass due to rotation.

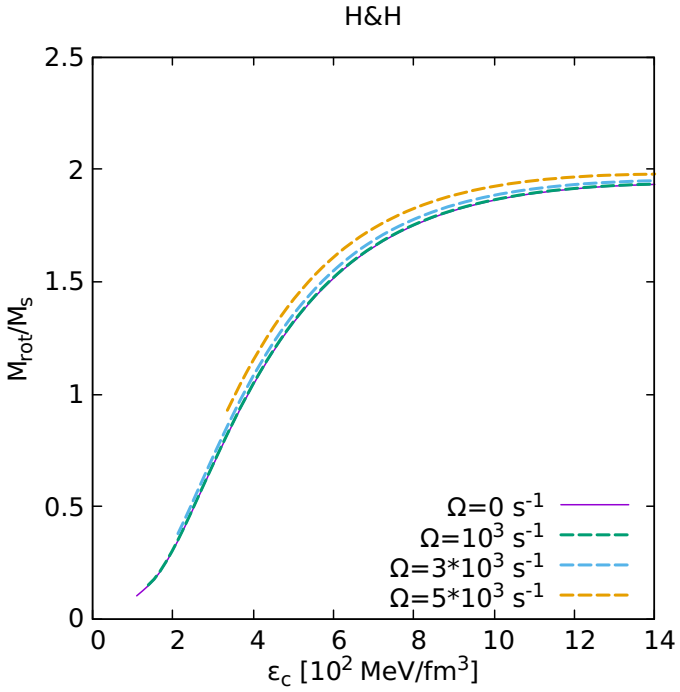

Figure 6.9: Rotational mass vs. central energy density for different angular frequencies Ω for the H&H EoS.

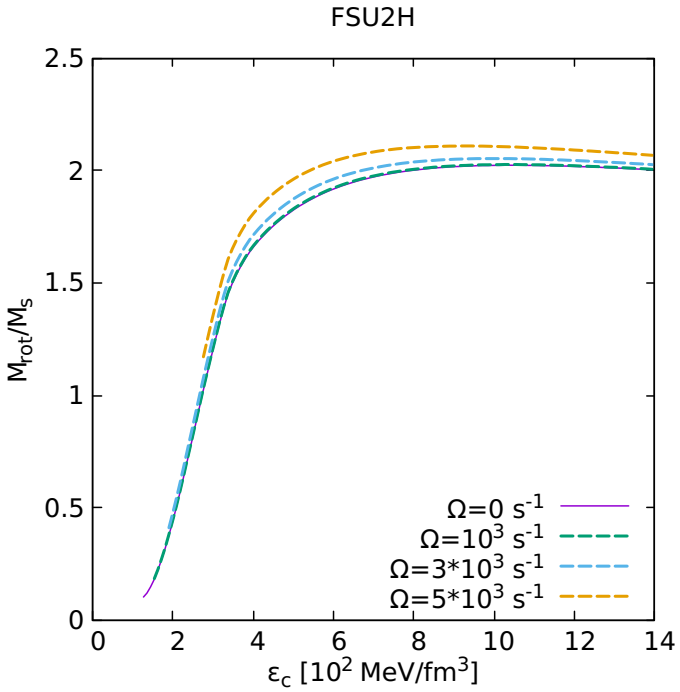

Figure 6.10: Rotational mass vs. central energy density for different angular frequencies Ω for the FSU2H EoS.

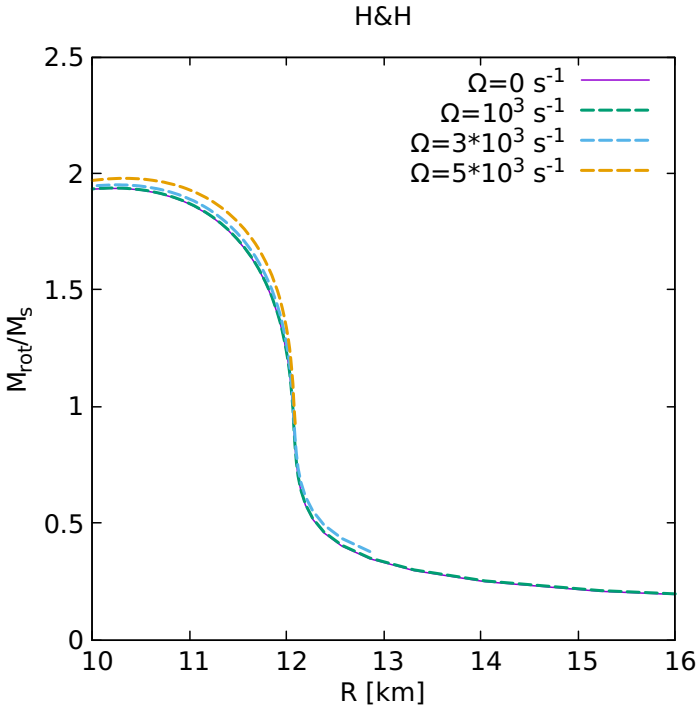

Figure 6.11: Rotational mass vs. radius for different angular frequencies Ω for the H&H EoS.

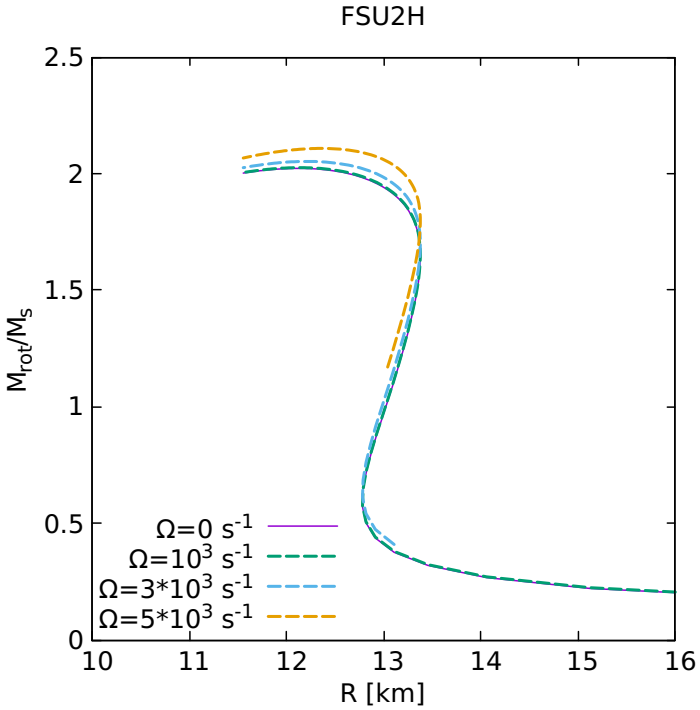

Figure 6.12: Rotational mass vs. radius for different angular frequencies Ω for the FSU2H EoS.

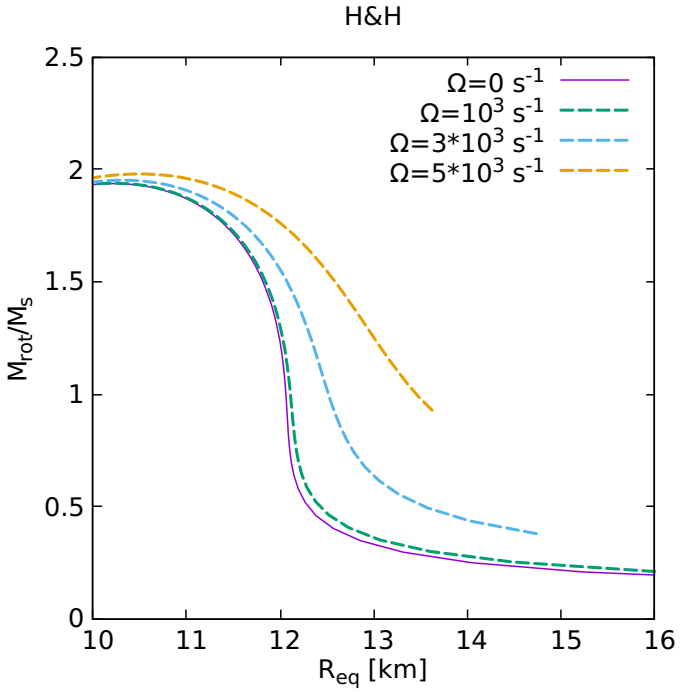

Figure 6.13: Rotational mass vs. equatorial radius for different angular frequencies Ω for the H&H EoS.

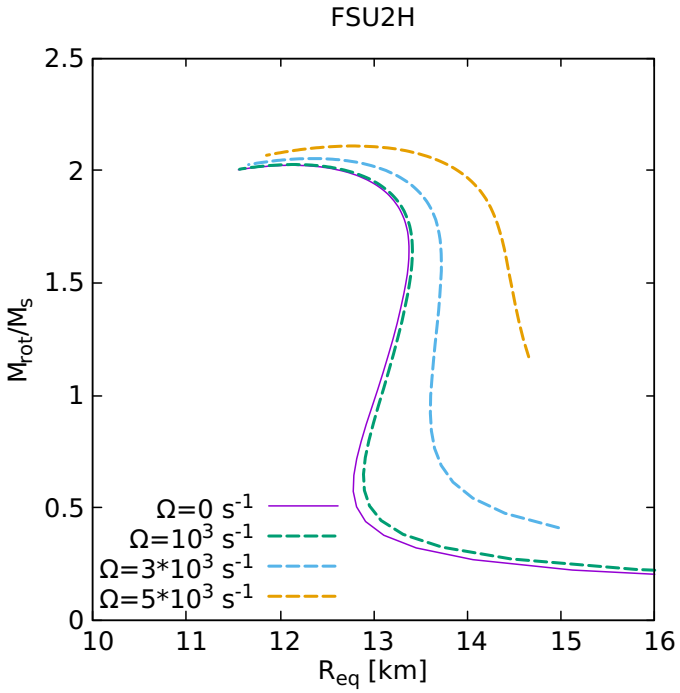

Figure 6.14: Rotational mass vs. equatorial radius for different angular frequencies Ω for the FSU2H EoS.

6.2.3 Moment of inertia

To finalise the study of rotating neutron stars, we have plotted the moment of inertia as a function of the rotational mass for different angular velocities for the H&H and FSU2H models in Figures 6.15 and 6.15, respectively.

From the previous mentioned figures, one can observe that the moment of inertia decreases for faster rotations. Moreover, it is also seen that as the mass of the star increases also does the moment of inertia. In particular, the FSU2H EoS gives rise to higher moment of inertia values in comparison to the H&H model due to its stiffer behaviour, which leads to larger-size stars.

Lastly, Figures 6.17 and 6.18 display the moment of inertia as a function of the equatorial radius for the different rotational frequencies and for the H&H and FSU2H models, respectively.

By the use of markers (crosses in Figures 6.17 and 6.18), we are able to compare stars with rotational masses of $1.5M_{\odot}$ for the different angular velocities and the two models. Consequently, we can conclude that the moment of inertia decreases with the rise of angular velocity, as already commented.

Keeping in mind that stars suffer an increment of mass when rotating, the rotating neutron stars with masses of $1.5M_{\odot}$ come from smaller gravitational masses and, hence, smaller central energy densities than the one associated to $1.5M_{\odot}$ non-rotating star. Moreover, considering that the increment of mass rises as angular velocity does, the rotating neutron star of $1.5M_{\odot}$ comes from an even smaller original star mass for faster rotation.

Therefore, these less massive non-rotating stars are described by larger radius in comparison with a more massive neutron star, giving rise to more diluted systems. Finally, those more diluted configurations explain the decrease of the moment of inertia with the angular velocity.

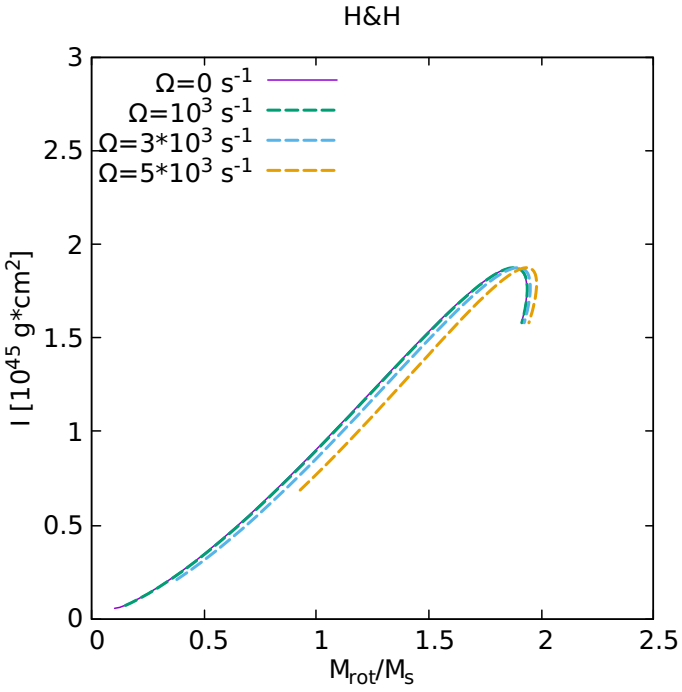

Figure 6.15: Moment of inertia vs. rotational mass for different angular frequencies Ω for the H&H EoS.

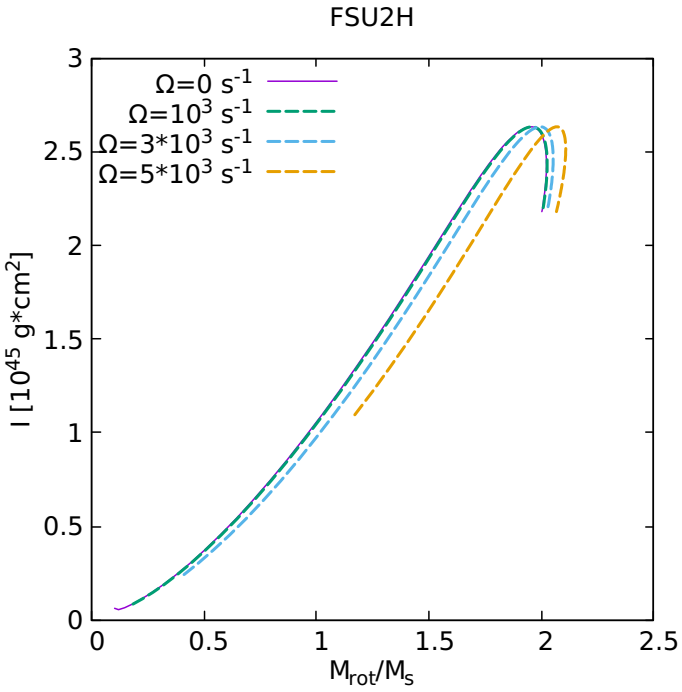

Figure 6.16: Moment of inertia vs. rotational mass for different angular frequencies Ω for the FSU2H EoS.

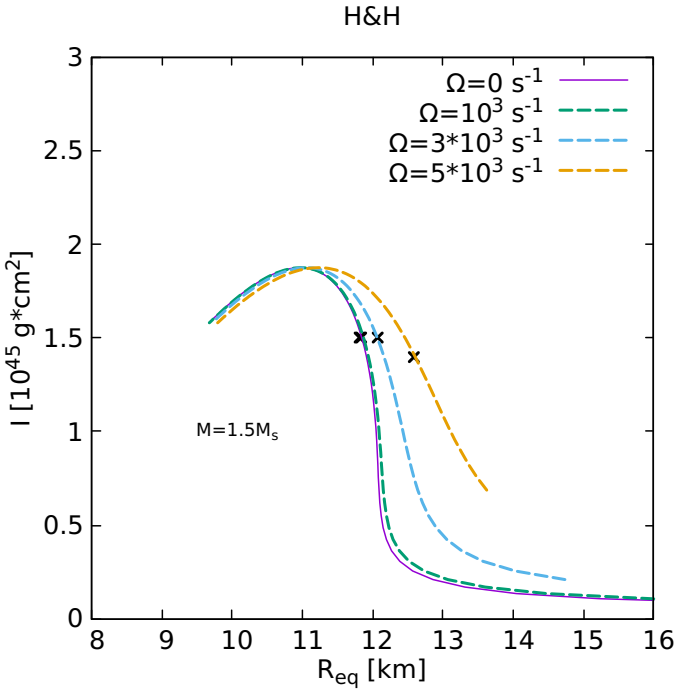

Figure 6.17: Moment of inertia vs. equatorial radius for different angular frequencies Ω for H&H EoS.

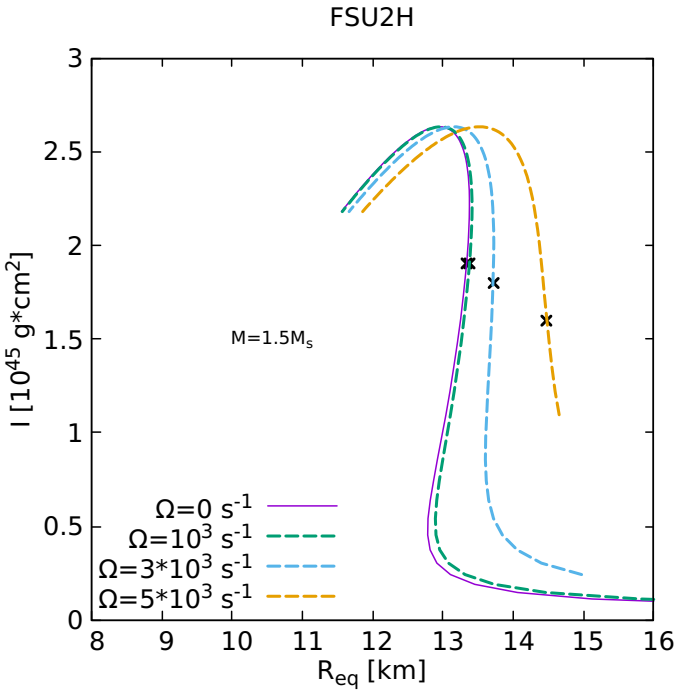

Figure 6.18: Moment of inertia vs. equatorial radius for different angular frequencies Ω for FSU2H EoS.

Chapter 7

Conclusions

The main aim of this project has been to study the rotation of neutron stars and to understand how it could affect to their mass, radius and moment of inertia. We have analysed the results obtained by the recently developed hyperonic FSU2H EoS and compared them with those of the nucleonic H&H model, being able to distinguish the differences in behaviour depending on the presence or absence of hyperons in the neutron star composition and, thus, arriving to diverse conclusions.

On the one hand, from the non-rotating neutron stars, one is able to foresee the behaviour due to rotation via the analysis of the EoS. A stiffer EoS is connected with characteristic higher gravitational masses and radii and, in consequence, smaller Keplerian frequencies. In this context, the Keplerian frequency sets the limit of angular velocity that a neutron star is capable to withstand. Thus, the FSU2H model due to its harder behaviour gives a sign of allowing lower rotational frequencies, leading of bigger affectations due to rotation.

On the other hand, from the rotating neutron stars, one is interested in the specific changes to their properties, such as the mass and radius. Thereby, rotating neutron stars characterised by smaller masses suffer larger deformations in radii than the more massive ones due to their lower Keplerian frequencies, leading to a more oblate configuration. Moreover, the faster the rotation, the larger the deformation and the increment of mass.

Referring to the moment of inertia of rotating neutron stars, the systems described by higher masses lead to larger values for the moment of inertia. When increasing the rotational frequency, we obtained a less intuitive result at first sight: the increment of the angular velocity leads to lower moment of inertia values, in spite of an increase of the equatorial radius.

Therefore, by comparing the H&H and FSU2H models, we have found that the hyperonic FSU2H model reaches a more oblate configuration due to rotation than the H&H EoS. This fact was previously predicted by its stiffer behaviour close to saturation densities that leads to larger radii deformations due to its distinctive smaller Keplerian frequencies. Additionally, the FSU2H EoS gives rise to more massive non-rotating neutron stars, larger rotational masses and, hence, higher moments of inertia.

Finally, in future projects, it would be interesting to calculate the tidal deformability of the rotating hyperonic neutron stars obtained. Furthermore, one must be intrigued from the very recent developed FSU2H model including Δ particles [34] as its analysis could be of great importance in understanding how neutron stars are affected to rotation. Thereby, we would be able to compare the rotating Δ neutron stars with the hyperonic ones already obtained.

Chapter 8

Bibliography

[1] Isaac Vidaña. A short walk through the physics of neutron stars, 2018.

[2] V. Kalogera and G. Baym. The maximum mass of a neutron star. *The Astrophysical Journal*, 470(1):L61–L64, Oct 1996.

[3] P. B. Demorest, T Pennucci, S. M. Ransom, M. S. E. Roberts, and J. W. T. Hessels. A two-solar-mass neutron star measured using Shapiro delay. *Nature*, 467:1081–1083, 10 2010.

[4] J Antoniadis, P. C. C. Freire, N Wex, T. M. Tauris, R. S. Lynch, M. H. van Kerkwijk, M Kramer, C Bassa, V. S. Dhillon, T Driebe, J. W. T. Hessels, V. M. Kaspi, V. I. Kondratiev, N Langer, T. R. Marsh, M. A. McLaughlin, T. T. Pennucci, S. M. Ransom, I. H. Stairs, J van Leeuwen, J. P. W. Verbiest, and D. G. Whelan. A Massive Pulsar in a Compact Relativistic Binary. *Science*, 340:448, 4 2013.

[5] H. Cromartie et al. A very massive neutron star: relativistic Shapiro delay measurements of PSR J0740+6620. 2019.

[6] J. M. Lattimer and M. Prakash. The Equation of State of Hot, Dense Matter and Neutron Stars. *Phys. Rept.*, 621:127–164, 2016.

[7] B. P. Abbott et al. GW170817: Observation of Gravitational Waves from a Binary Neutron Star Inspiral. *Phys. Rev. Lett.*, 119(16):161101, 2017.

[8] Ben Margalit and Brian D. Metzger. Constraining the maximum mass of neutron stars from multi-messenger observations of gw170817. *The Astrophysical Journal*, 850(2):L19, Nov 2017.

[9] S. Woosley and T. Janka. The physics of core-collapse supernovae. *Nature Physics*, 1(1):147–154, Dec 2005.

[10] L. Tolos, M. Centelles, and A. Ramos. The Equation of State for the Nucleonic and Hyperonic Core of Neutron Stars. *Publ. Astron. Soc. Austral.*, 34:e065, 2017.

[11] M. Heiselberg, H.and Hjorth-Jensen. Phases of dense matter in neutron stars. *Phys. Rept.*, 328:237–327, 2000.

[12] [Glendenning]_Compact_stars(BookFi).

[13] Wikipedia. White Dwarf.

[14] J. R. Oppenheimer and G. M. Volkoff. On massive neutron cores. *Phys. Rev.*, 55:374–381, Feb 1939.

[15] R. C. Tolman. Static solutions of einstein's field equations for spheres of fluid. *Phys. Rev.*, 55:364–373, Feb 1939.

[16] B.K. Harrison, M. Wakano and J.A. Wheeler. *Matter-energy at high density: end point of thermonuclear evolution.* La structure et évolution de l'univers, R. Stoops, Bruxelles, 1958.

[17] A. G. W. Cameron. Pycnonuclear reations and nova explosions. *The Astrophysical Journal*, 130:916, Nov 1959.

[18] R. A. Wolf. Some Effects of the Strong Interactions on the Properties of Neutron-Star Matter. *The Astrophysical Journal*, 145:834, Sep 1966.

[19] D. Pines and M. A. Alpar. Superfluidity in neutron stars. *Nature*, 316:27–32, Jul 1985.

[20] J. M. Lattimer. Viewpoint: A Rapidly Cooling Neutron Star.

[21] J. N. Bahcall and R. A. Wolf. Neutron stars. ii. neutrino-cooling and observability. *Phys. Rev.*, 140:B1452–B1466, Dec 1965.

[22] J. N. Bahcall and R. A. Wolf. An Observational Test of Theories of Neutron-Star Cooling. *The Astrophysical Journal*, 142:1254–1256, October 1965.

[23] F. Pacini. Energy Emission from a Neutron Star. *Nature*, 216:567–568, Nov 1967.

[24] Bell S. J. Pilkington J. D. H. Scott P. F. Collins R. A. Hewish, A. Observation of a Rapidly Pulsating Radio Source. *Nature*, 217:709–713, Feb 1968.

[25] T. Gold. Rotating Neutron Stars and the Nature of Pulsars. *Nature*, 221:25–27, Jan 1969.

[26] S. Rappaport and P. C. Joss. Binary x-ray pulsars. *Nature*, 266:123–125, Mar 1977.

[27] R. A. Hulse and J. H. Taylor. Discovery of a pulsar in a binary system. *The Astrophysical Journal Letters*, 195:L51–L53, January 1975.

[28] D G Yakovlev P. Haensel, A.Y. Potekhin. *Neutron Stars 1. Equation of State and Structure*, volume 326. Springer, 2007.

[29] J. A. Pons, D. Vigano, and N. Rea. Too much "pasta" for pulsars to spin down. *Nature Phys.*, 9(arXiv:1304.6546):431–434, Apr 2013.

[30] W. G. Newton. A taste of pasta?, Jun 2013. Nature Publishing Group, a division of Macmillan Publishers Limited. All Rights Reserved.

[31] J. B. Hartle. Slowly rotating relativistic stars. i. equations of structure. *Astrophys. J.*, 150:1005, 1967.

[32] J. B. Hartle and K. S. Thorne. Slowly Rotating Relativistic Stars. II. Models for Neutron Stars and Supermassive Stars. *Astrophys. J.*, 153:807, September 1968.

[33] M. Salgado, S. Bonazzola, E. Gourgoulhon, and P. Haensel. High precision rotating netron star models 1: Analysis of neutron star properties. , 291:155–170, November 1994.

[34] P. Ribes, A. Ramos, L. Tolos, C. Gonzalez-Boquera, and M. Centelles. Interplay between delta particles and hyperons in neutron stars. *The Astrophysical Journal*, 883(2):168, Oct 2019.

Appendix A

Appendix

A.1 Programme

```
c... Program that solves the TOV equations for a given EoS and the Hartle-Thorne
     approach for rotating neutron stars
c... Determines M-R diagram
c... Gives Mass profile for a couple of stars
c... Gives rotation parameters and characterises the rotational deformation of the
     star
c... (Adpated by Anna Campoy from Àngels Ramos and Laura Tolós code of non-rotating
     neutron stars)

      IMPLICIT NONE
      integer i,ncrust,ncore,ni,nf,nmax,nstep,k,ipre,ndiscard,imax
      integer column
      parameter (nmax=5000)
      real*8 pai,pai2,conv1,conv2,conv3,conv4,conv5,conv6,conv7
      real*8 pmn,msolar,mmax,rmax
      real*8 rho(nmax),en(nmax),pre(nmax),eder(nmax)
      real*8 nur(100000),w(100000),mass(100000),press(100000)
      real*8 functh2(100000),functv2(100000)
      real*8 eps0(100000),eps2(100000),press2(100000)
      real*8 derj(100000),derw(100000),dernu(100000)
      real*8 m1,p1,en1,dens1,fntv1,dx,nu0,w0,w1,fntj1,mass1,press1
      real*8 functv2_1, functh2_1,v2,h2,eder0,eder1
      real*8 derw1,derj1,dernu1
      real*8 ma,prener,ener,x,dens,fntv,fntvR,fntj,mass0,press0
      real*8 dm,dp,dv,fac1,fac2,jintx,dmass0,dpress0,dh2,dv2
      real*8 omega,wconst,omega_arb,Jsum,inmom,massinc
      real*8 polarR,equatR,eccent,kepler
      real*8 xx
      real*8 premin
```

```
c... input files
      open(unit=7,file='EoS_crust_FSU2H_reduced.dat')
c... output files
      open(unit=8,file='M_vs_R_npe.dat')
      open(unit=9,file='profile_npe1.dat')
      open(unit=10,file='profile_npe2.dat')
      open(unit=12,file='profile_npe3.dat')
      open(unit=11,file='derederp.dat')
      write(11,'(a)') '#rho      e       p       de/dp'
      open(unit=13,file='M_vs_R_rot.dat')
      open(unit=14,file='M_vs_R_rot-monopole.dat')
      open(unit=15,file='M_vs_R_rot-def.dat')
      open(unit=17,file='w(i).dat')
      open(unit=18,file='usefull_parameters.dat')

c... conversion factors
      pai=3.14159
      pai2=pai*pai
      mmax=0.d0
      rmax=0.d0
      conv1=1.3234d-16 !(cm^(-2))*(fm^3/MeV) [de Mev/fm^3 a cm^(-2)]
      conv2=1.d-5 !km/cm [de cm a Km]
      conv3=1.d39 !fm^3/cm^3 [de fm^-3 a cm^-3]
      conv4=7.4237d-29 ! [g/cm^3 a cm^(-2)] (1g a cm)
      conv5=2.9979d10 !1s a cm
      conv6=4.0383d38 ! conv5/conv4  [cm a g.cm/s]
      conv7=1.d-15 !cm3 a km3
      pmn=939.566d0 !MeV
      msolar=1.4766d5 !cm
      omega=0./conv5 !cm^(-1)
      column=0

c... write in file radius and mass
      write(8,'(2a)') '#r(km),         M/Msol,       rho_c(fm-3),',
     &         '  E_c(MeV/fm^3),      nu (adim),      index'

c... write in file metric function, j function, dragging angular velocity,
     arbitrary angular velocity, total angular momentum and inertial momentum
      write(13,'(3a)') '#r(km),       M/Msol,         nu(adim),',
     &               '     j(adim),      w(s-1),    Omega_arb(s-1),',
     &             '  J (g*cm^2/s),  I(g*cm^2),   kepler(s^-1)    index'
```

```
c... write in file monopole mass and pressure, v2 and h2 functions, and the
     increase of mass due to rotation
      write(14,'(3a)') '#r(km),       M/Msol,  monopole mass(g)',
     &           '    monopole pressure,      v2 function,',
     &           '      h2 function,    massinc(g),        index'

c... write in file quadrupole pressure, spherical and quadrupole stretching
     functions, polar and equatorial radius, and eccentricity
      write(15,'(3a)') '#r(km),       M/Msol,     quadr pressure,',
     &           ' sph stretch(cm),   quadr stretch(cm),  polar R(km),',
     &           '  equatorial R(km),        eccentricity,        index'
c... write in file rel. ang. velocity and Kepler frequency
      write(17,'(2a)') '#r(km),         M/Msol,       w(i)/omega,',
     &         '      kepler(s^-1),      index'

c... write in file rotational mass, polar and equatorial radius, Kepler freq.,
     eccentricity, central energy density and moment of inertia
      write(18,'(3a)') '  #r(km),       M/Msol,      M/Msol rot,',
     &         '     Req(km),    Rpol(km),    kepler(s^-1),   eccent,',
     &      '  E_c(MeV/fm^3),      I(g*cm^2),     index'


c... read files of density, energy density and presure (crust and core)
      ncrust=129
      ncore=108
      nf=ncrust+ncore !total number of points

      read(7,*) !read the points of the EoS file

      do i=1,nf
        read(7,*) xx,en(i),pre(i) !rho: fm^-3, en: MeV/fm^3, pre: MeV/fm^3
        rho(i)=xx*conv3 !cm^(-3)
c... write(*,*) rho(i)/conv3,en(i),pre(i)
        en(i)=en(i)*conv1    !cm^(-2)
        pre(i)=pre(i)*conv1  !cm^(-2)
      enddo

c...  computing derivative of energy density w.r.t pressure density
      do i=1,nf-1
        eder(i)=(en(i+1)-en(i))/(pre(i+1)-pre(i))
        if(pre(i+1).eq.pre(i)) eder(i)=eder(i-1)
c        if(i.eq.ncrust) eder(i)=eder(i-1)
      enddo
      eder(nf)=eder(nf-1) !set last value equal of the derivative to the previous one
```

```
      write(11,'(4g20.12)') rho(1)/conv3,en(1)/conv4,pre(1)/conv4,
     &                      eder(1)
      do i=2,nf-1
        if(i.eq.83.or.i.eq.ncrust.or.eder(i).lt.0.d0)
     &        eder(i)=eder(i-1)+(eder(i+1)-eder(i-1))*(rho(i)-rho(i-1))/
     &                         (rho(i+1)-rho(i-1))

      write(11,'(4g20.12)') rho(i)/conv3,en(i)/conv4,pre(i)/conv4,
     &                      eder(i)
      enddo
      write(11,'(4g20.12)') rho(nf)/conv3,en(nf)/conv4,pre(nf)/conv4,
     &                      eder(nf)

c      stop

      premin=pre(1)

c... step for integration of Euler method
      nstep=100000 !with step of 1 meter, we go up to 100 Km
      dx=100 !cm (step of 1 meter)

c... which initial/central pressure to use to calculate the corresponding mass-radius
      ni=ncrust+2 !where to start

c... loop over different stars (with different central densities)
      do k=ni,nf
c      do k=213,213

c... m1: initial mass; p1: initial pressure; en1: initial energy density;
     dens1: initial density; fntv1: initial nu function
        m1=0.d0 !initial mass
        p1=pre(k) !initial pressure
        en1=en(k) !initial energy density
        dens1=rho(k) !initial density
        fntv1=0.d0 !initial metric function
c... write(*,*) k, p1/conv1,en1/conv1,dens1/conv3

c... solve differential equations with Euler method
c... starting values
        ma=m1
        prener=p1
        ener=en1
        dens=dens1
        fntv=fntv1
        x=1 !cm
```

```
        if (k.eq.2581)
     & write(9,'(3a)') '#r(km),       M/Msol,         P/c^2(g/cm^3),',
     &                 '       E/c^2(g/cm^3),        dens(fm-3),',
     &                 '      nu (adim)'
        if (k.eq.2627)
     & write(10,'(3a)') '#r(km),       M/Msol,         P/c^2(g/cm^3),',
     &                 '       E/c^2(g/cm^3),        dens(fm-3),',
     &                 '      nu (adim)'
        if (k.eq.2572)
     & write(12,'(3a)') '#r(km),       M/Msol,         P/c^2(g/cm^3),',
     &                 '       E/c^2(g/cm^3),        dens(fm-3),',
     &                 '      nu (adim)'

c... start integration (outwards)
        do i=1,nstep

c... write density profile for a couple of cases (M=1.4Msolar, M=Mmax=1.9Msolar,
     M=Msolar)
        if (k.eq.2581)
     & write(9,'(6g20.12)') x*conv2,ma/msolar,prener/conv4,ener/conv4,
     &                      dens/conv3,fntv
        if (k.eq.2627)
     & write(10,'(6g20.12)') x*conv2,ma/msolar,prener/conv4,ener/conv4,
     &                       dens/conv3,fntv
        if (k.eq.2572)
     & write(12,'(6g20.12)') x*conv2,ma/msolar,prener/conv4,ener/conv4,
     &                       dens/conv3,fntv

c... description of differential TOV equations and metric function
          dm=4.*pai*x**2.*ener*dx ! cm
          dp=-(ener+prener)*(ma+4.*pai*x**3.*prener)/(x*(x-2.*ma))*dx !cm^(-2)
          dv=(ma+4.*pai*x**3.*prener)/(x*(x-2.*ma))*dx !adim

c... new mass, pressure, radial position and metric function
          ma=ma+dm
          prener=prener+dp
          x=x+dx
          fntv=fntv+dv

c... write(*,*) ma/msolar,prener/conv4,x*conv2,fntv

          if(prener.lt.premin) then  !if pressure less than minimum --> finish the loop
          ma=ma-dm
          x=x-dx
          prener=prener-dp
```

```
          fntv=fntv-dv
          goto 10
          endif

c... determine index of new pressure within the pressure array
          do ipre=1,nf-1
          if(((prener-pre(ipre))*(prener-pre(ipre+1))).lt.0.) goto 11
          enddo
 11       continue

c... linear interpolation (to determine energy and density at the new position)
          ener=en(ipre)+(en(ipre+1)-en(ipre))/(pre(ipre+1)-pre(ipre))*
     &              (prener-pre(ipre))
          dens=rho(ipre)+(rho(ipre+1)-rho(ipre))/(pre(ipre+1)-pre(ipre))*
     &              (prener-pre(ipre))
c...

          enddo  ! enddo nstep integration

        write(8,*) '#no solution for k:',k
        write(*,*) '#no solution for k:',k
        write(8,'(5g14.6,i5)') x*conv2,ma/msolar,dens1/conv3,en1/conv1,
     & fntv,k
c...     write(*,'(3g14.6,i5)') x*conv2,ma/msolar,dens1/conv3,k

        goto 12

 10     continue

        write(8,'(5g14.6,i5)') x*conv2,ma/msolar,dens1/conv3,en1/conv1,
     &  fntv,k
c...    write(*,'(3g14.6,i5)') x*conv2,ma/msolar,dens1/conv3,k

c     max mass, and radius at the max mass
        if (ma/msolar.gt.mmax) then
          mmax = ma/msolar
          rmax = x*conv2
        endif

c ... solve Hartle-Thorne approach: rotation neutron stars eqs
c ... new initial conditions
        fntvR=fntv !assign nu final value as nu(R)
        nu0=-fntvR+0.5*LOG(1.-2.*ma/x) ! new initial condition for the metric function
                                        (match with the exterior solution)
c        print *, ' nu0=',nu0
        m1=0.d0 !initial mass
```

```
        p1=pre(k) !initial pressure
        en1=en(k) !initial energy density
        dens1=rho(k) !initial density
        fntv1=nu0 !initial metric function
        w0=1.d0 !1rst boundary condition to dragging angular velocity (arb. cte value)
        w1=w0 !2nd boundary cond. to dragg. ang. vel. (1rst derivative equal to 0 at r=0)
        fntj1=EXP(-nu0) !1rst value of j function
        Jsum=0.d0 !initial total angular momentum

c... solve differential equations with Euler method
c... starting values
        ma=m1
        prener=p1
        ener=en1
        dens=dens1
        fntv=fntv1
        x=1 !cm

c... once solved the TOV eqs, open new integration loop to solve rotation eqs
        do i=1,nstep

          dm=4.*pai*x**2.*ener*dx ! cm^(-2)*cm
          dp=-(ener+prener)*(ma+4.*pai*x**3.*prener)/(x*(x-2.*ma))*dx !cm^(-3)*cm
          dv=(ma+4.*pai*x**3.*prener)/(x*(x-2.*ma))*dx !dimentionless

c... new mass, preassure, radius and metric function
          ma=ma+dm
          prener=prener+dp
          x=x+dx
          fntv=fntv+dv
          nur(i)=fntv

c... write(*,*) ma/msolar,prener/conv4,x*conv2,fntv

          fntj=EXP(-fntv)*(1.-2.*ma/x)**(0.5) ! j function value for every integration
                                              step in r (dimentionless)
c        print *, ' fntj=',fntj
c        print *, ' fntv=',nur(i)
c        print *, ' ma=',ma/msolar

c... defining derivative of j function, derivative of metric function and
     factor1 and factor2 for diff eq (5.2)
          derj(i)=(fntj-fntj1)/dx
          dernu(i)=(nur(i)-fntv1)/dx
          fac1=fntj+4.*fntj*dx/x+derj(i)*dx+4.*derj(i)*dx**2./x
          fac2=2.*fntj+4.*fntj*dx/x+derj(i)*dx
```

```
          w(i)=(-fntj*w0+fac2*w1)/fac1 !diff. eq. we want to solve for dragg. ang. vel.
          derw(i)=(w(i)-w1)/dx ! derivative of dragging angular velocity
          jintx=8.*(pai/3.)*x**4.*((prener+ener)/(1.-2.*ma/x)**(0.5))*
     &    w(i)*EXP(-fntv) !integrand of total angular momentum eq

          Jsum=Jsum+dx*jintx !total angular momentum integral

c... we proceed as previous loop and finalize when pressure is less than minimum value
          if(prener.lt.premin) then  ! set previous values
          ma=ma-dm
          x=x-dx
          prener=prener-dp
          imax=i-1 !last valid number of the integration loop
          nur(imax)=fntv-dv
          w(imax)=w1
          derw(imax)=derw1
          derj(imax)=derj1
          dernu(imax)=dernu1
          Jsum=Jsum-dx*jintx
          fntj=fntj1
          goto 20
          endif

c... determine index of new pressure within the pressure array
          do ipre=1,nf-1
          if(((prener-pre(ipre))*(prener-pre(ipre+1))).lt.0.) goto 21
          enddo
 21       continue

c... linear interpolation (to determine energy at the new position)
          ener=en(ipre)+(en(ipre+1)-en(ipre))/(pre(ipre+1)-pre(ipre))*
     &              (prener-pre(ipre))

c... assign "i" find value as "i-1" value, continue with the loop
        fntj1=fntj
        w0=w1
        w1=w(i)
        derw1=derw(i)
        derj1=derj(i)
        dernu1=dernu(i)

c      write(13,'(6g20.12)') x,ma,fntv,fntj,w(i),Jsum

         enddo !end nstep integration
```

```
 20     continue

c... calculation of the angular velocity at r=R (outside the star)
        omega_arb=w1+2.*Jsum/x**3.
        wconst=omega/omega_arb !constant value in order to rescale dragging angular
                               velocity if desired

c... write without applying normalization of wconst
c        write(13,'(7g25.16,i5)') x*conv2,ma/msolar,nur(imax),fntj1,
c     &                           w1*conv5,Jsum*conv6,omega_arb*conv5,k
c      write(*,'(5g14.6,i5)') x*conv2,ma/msolar,fntv,fntj,w,k

c... rescale dragging angular velocity, its derivative and angular total momentum
     to omega desired value
        do i=1,imax
          w(i)=wconst*w(i) ! cm^(-1)
          derw(i)=wconst*derw(i) ! cm^(-1)
        enddo

        Jsum=Jsum*wconst ! cm^2
        inmom=Jsum/omega ! cm^3
        kepler=0.65*(ma/x**3)**0.5 !cm^(-1)


c... write applying normalization of wconst
        write(13,'(9g14.6,i5)') x*conv2,ma/msolar,nur(imax),fntj1,
     &                          w(imax)*conv5,omega_arb*conv5,
     &                          Jsum*conv6,inmom/conv4,kepler*conv5,k

c... reset initial conditions for a new loop
        m1=0.d0 !initial mass
        p1=pre(k) !initial pressure
        en1=en(k) !initial energy density
        if(pre(k+1).eq.pre(k)) then !conditions to the dervivative of energy density
                                       w.r.t. pressure density
          eder1=(en(k)-en(k-1))/(pre(k)-pre(k-1))
        else
          eder1=(en(k+1)-en(k))/(pre(k+1)-pre(k))
        endif
c... write every of these energy density w.r.t. preassure density derivatives into
     an array pf k dimention
        eder1=eder(k)

c... write(*,*) k, p1/conv1,en1/conv1,dens1/conv3
```

```
c... solve differential equations with Euler method
c... new starting values
        ma=m1
        prener=p1
        ener=en1
        mass0=0.d0 !initial monopole mass  [cm]
        eder0=eder1 ! initial de/dp value [dimentionless]
        press0=0.d0 !initial monopole pressure [dimentionless]
        h2=0.d0 !boundary condition to h2 function [dimentionless]
        v2=0.d0 !boundary condition to v2 function [dimentionless]
        x=1 ! cm

c... initialising integration loop in order to solve eqs 42 & 43
        do i=1,imax

          dm=4.*pai*x**2.*ener*dx ! cm
          dp=-(ener+prener)*(ma+4.*pai*x**3.*prener)/(x*(x-2.*ma))*dx ! cm^(-2)

          fntj=EXP(-nur(i))*(1.-2.*ma/x)**(0.5) ! j function value for every
                                                  integration step in r

          dmass0=(4*pai*x**2*eder0*(ener+prener)*press0+1/12.*fntj**2*
     &            x**4*(derw(i))**2+8.*pai/3.*x**5*fntj**2*
     &            ((ener+prener)/(x-2*ma))*(w(i))**2)*dx
          dpress0=(-(1.+8.*pai*x**2*prener)/((x-2*ma)**2)*mass0-
     &             4.*pai*((prener+ener)*x**2)/(x-2*ma)*press0+
     &             1./12.*(x**4*fntj**2)/(x-2*ma)*(derw(i))**2+
     &             1./3.*((3.*x**2*fntj**2*w(i)**2)/(x-2*ma)+
     &             (x**3*2.*fntj*derj(i)*w(i)**2)/(x-2*ma)+
     &             (x**3*fntj**2*2.*w(i)*derw(i))/(x-2*ma)-
     &             (x**3*fntj**2*w(i)**2)*(1-2*dm/dx)/(x-2*ma)**2))*dx
          dh2=((-2.*dernu(i)+2.*x/((x-2*ma)*dernu(i))*(2.*pai*
     &        (ener+prener)-ma/x**3))*h2-2/(x*(x-2*ma)*dernu(i))*v2+
     &        1./6.*(x*dernu(i)-1./(2.*(x-2*ma)*dernu(i)))*x**3*fntj**2*
     &         (derw(i))**2-1./3.*(x*dernu(i)+ 1./(2*(x-2*ma)))/
     &         dernu(i)*x**2*w(i)**2*2.*fntj*derj(i))*dx

          dv2=(-2.*dernu(i)*h2+(1./x+dernu(i))*(-x**3/3*2.*fntj*derj(i)*
     &         w(i)**2+fntj**2/6.*x**4*(derw(i))**2))*dx

c ... new mass, preassure, radius, monopole mass and pressure, v2 and h2 functions
          ma=ma+dm
          prener=prener+dp
          x=x+dx
          mass0=mass0+dmass0
```

```
          press0=press0+dpress0
          h2=h2+dh2
          v2=v2+dv2
          mass(i)=mass0 ! defining monopole mass array
          press(i)=press0 ! defining monopole pressure array
          functv2(i)=v2 ! defining v2 function array
          functh2(i)=h2 ! defining h2 function array

c... write(*,*) ma/msolar,prener/conv4,x*conv2,fntv

c... determine index of new pressure within the pressure array
          do ipre=1,nf-1
          if(((prener-pre(ipre))*(prener-pre(ipre+1))).lt.0.) goto 31
          enddo
 31       continue

c... linear interpolation (to determine energy and density at the new position)
          ener=en(ipre)+(en(ipre+1)-en(ipre))/(pre(ipre+1)-pre(ipre))*
     &              (prener-pre(ipre))

c... linear interpolation (to determine energy derivative w.r.t. pressure
     at the new position)
          eder0=eder(ipre)+
     &          (eder(ipre+1)-eder(ipre))/(pre(ipre+1)-pre(ipre))*
     &          (prener-pre(ipre))

c... write interesting parameters in order to make some figures
         write(17,'(4g25.16,i5)') x*conv2,ma/msolar,w(i)/omega,
     &   kepler*conv5,k
c        print *, ' mass0=',mass0
c        print *, 'press0=',press0

        enddo

c... increase of mass of the star due to rotation
        massinc=mass(imax)+Jsum**2/x**3 ! cm

        write(14,'(7g14.6,i5)') x*conv2,ma/msolar,mass(imax)/conv4,
     &                          press(imax),functv2(imax),functh2(imax),
     &                          massinc/msolar,k

c... outside the star, relative angular velocity behaves as:
        do i=imax+1,imax+8000
         x=x+dx
          w(i)=omega-2.*Jsum/x**3
         write (17,*) x*conv2,column,w(i)/omega
```

```
        enddo

c ... initialising again the loop
        m1=0.d0 !initial mass
        p1=pre(k) !initial pressure
        en1=en(k) !initial energy density

c... write(*,*) k, p1/conv1,en1/conv1,dens1/conv3

c... solve differential equations with Euler method
c... initial conditions
        ma=m1
        prener=p1
        ener=en1
        x=1 !cm

c ... initialising integration loop in order to solve eqs 49 & 50
        do i=1,imax

          dm=4.*pai*x**2.*ener*dx ! cm
          dp=-(ener+prener)*(ma+4.*pai*x**3.*prener)/(x*(x-2.*ma))*dx ! cm^(-2)

c... new mass, pressure and radial position
          ma=ma+dm
          prener=prener+dp
          x=x+dx

c... definition of quadrupole pressure perturbation array, and spherical
     and quadrupole stretching function arrays
          press2(i)=-functh2(i)-1./3.*x**2*w(i)**2*EXP(-2*nur(i)) ! dimentionless
          eps0(i)=-press(i)*(prener+ener)*dx/dp ! cm
          eps2(i)=-press2(i)*(prener+ener)*dx/dp ! cm

c... determine index of new pressure within the pressure array
          do ipre=1,nf-1
          if(((prener-pre(ipre))*(prener-pre(ipre+1))).lt.0.) goto 41
          enddo
 41       continue

c... linear interpolation (to determine energy at the new position)
          ener=en(ipre)+(en(ipre+1)-en(ipre))/(pre(ipre+1)-pre(ipre))*
     &              (prener-pre(ipre))


        enddo
```

```
c... gives polar and equatorial radius, and eccentricity (description of the
     star's shape at its surface)
        equatR=x+eps0(imax)-eps2(imax)/2. ! cm
        polarR=x+eps0(imax)+eps2(imax) ! cm
        eccent=(1-(polarR/equatR)**2)**0.5 ! dimentionless

        write(15,'(8g14.6,i5)') x*conv2,ma/msolar,press2(imax),
     &                          eps0(imax),eps2(imax),polarR*conv2,
     &                          equatR*conv2,eccent,k

        write(18,'(9g14.6,i5)') x*conv2,ma/msolar,(ma+massinc)/msolar,
     &                          equatR*conv2,polarR*conv2,kepler*conv5,
     &                          eccent,en1/conv1,inmom/conv4,k

 12     continue

      enddo !k different central densities

c... write maximum mass and the corresponding radius
      open(unit=22, file='M_R_max_grav-pr.res')
      print*, mmax, rmax
      write(22,*) 'Mmax        Rmax'
      write(22,'(2g14.6)') mmax,rmax

      close(5)
      close(7)
      close(8)
      close(9)
      close(10)
      close(12)
      close(13)
      close(14)
      close(15)
      close(17)
      close(22)
      end
```